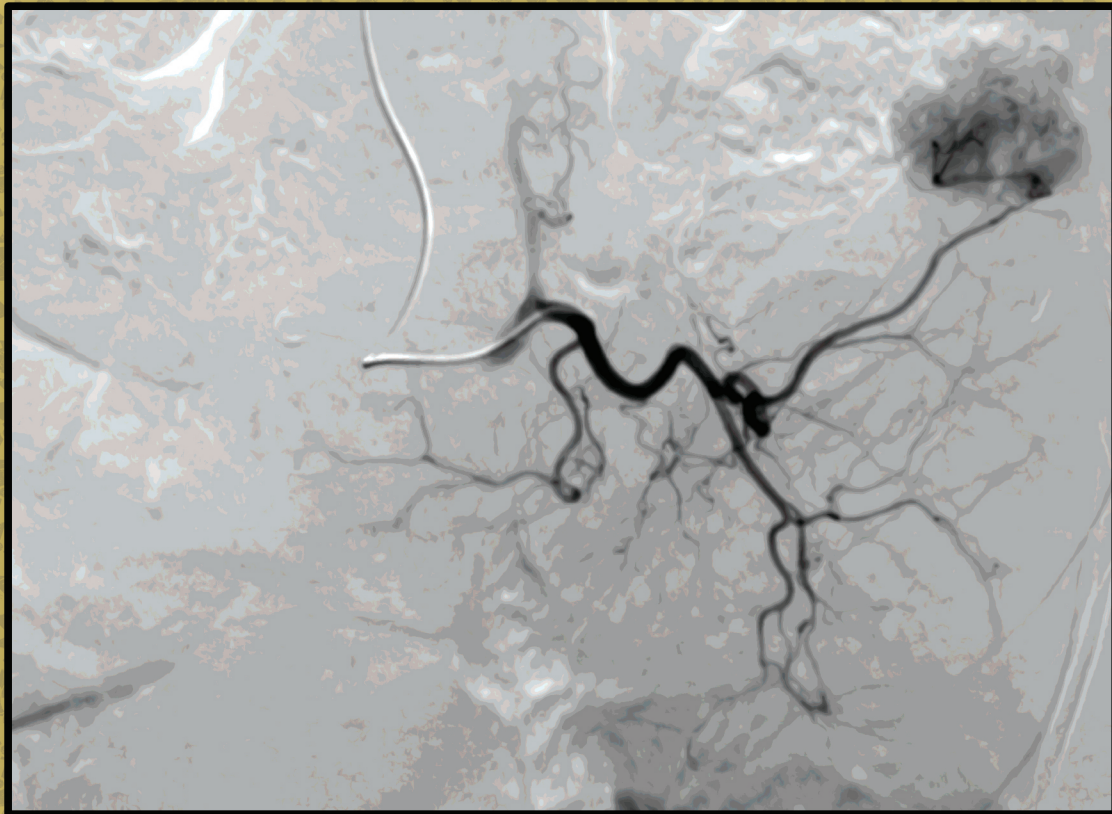


Master Thesis

Evaluation of Radiation Dose to the Eye Lens and Head of Interventional Radiologists

Psarras Michail

R.N.:20160069



Supervisors

Professor of Medical Radiation Physics, DUTH

I. Seimenis

Professor of Medical Radiation Physics, NKUA

E. P. Efstathopoulos

Athens 2018

To my memorable

Father...

ΠΡΟΛΟΓΟΣ

Η παρούσα διπλωματική εργασία εκπονήθηκε στα πλαίσια του Διαπανεπιστημιακού- Διατμηματικού Προγράμματος Μεταπτυχιακών Σπουδών στην Ιατρική Φυσική- Ακτινοφυσική της Ιατρικής Σχολής του Εθνικού και Καποδιστριακού Πανεπιστημίου Αθηνών (ΕΚΠΑ) σε συνεργασία με το Τμήμα Ιατρικής του Δημοκρίτειου Πανεπιστημίου Θράκης (ΔΠΘ). Η τριμελής εξεταστική επιτροπή ορίστηκε ως εξής:

- **Ιωάννης Σειμένης** Καθηγητής Ιατρικής Φυσικής, Ιατρική σχολή ΔΠΘ.
- **Ευστάθιος Ευσταθόπουλος** Καθηγητής Ιατρικής Φυσικής, Ιατρική σχολή ΕΚΠΑ
- **Σταύρος Σπηλιόπουλος** Επίκουρος Καθηγητής Επεμβατικής Ακτινολογίας, Ιατρική σχολή ΕΚΠΑ

Η διεκπεραίωση της διπλωματικής εργασίας πραγματοποιήθηκε στο Β΄ Εργαστήριο Ακτινολογίας του Πανεπιστημιακού Γενικού Νοσοκομείου Αττικών και στο Τμήμα Δοσιμετρίας και Βαθμονομήσεων της Ελληνικής Επιτροπής Ατομικής Ενέργειας (ΕΕΑΕ).

ΕΥΧΑΡΙΣΤΙΕΣ

Ξεκινώντας θα ήθελα να ευχαριστήσω τους υπεύθυνούς μου κ. Ιωάννη Σειμένη και κ. Ευστάθιο Ευσταθόπουλο για την πολύτιμη καθοδήγηση, εμπιστοσύνη, εκτίμηση και ευκαιρία που μου δώσανε για να φέρω εις πέρας τη παρούσα διπλωματική εργασία. Στη συνέχεια, θα ήθελα να ευχαριστήσω θερμά την ερευνήτρια και υποψήφια Διδάκτορα κ. Αγάπη Πλουσή, για όλες τις συμβουλές και τη βοήθεια που μου πρόσφερε και κυρίως για όλες εκείνες τις στιγμές που ανέχτηκε και διαχειρίστηκε το άγχος μου. Επίσης, θέλω να ευχαριστήσω την υπεύθυνη του Τμήματος Δοσιμετρίας και Βαθμονομήσεων της ΕΕΑΕ κ. Ελευθερία Καρίνου, καθώς επίσης και τον κ. Παναγιώτη Ασκούνη. Ακόμα, θα ήθελα να ευχαριστήσω τον Καθηγητή Επεμβατικής Ακτινολογίας του ΕΚΠΑ κ. Ηλία Μπρούντζο, τον Αναπληρωτή καθηγητή Επεμβατικής Ακτινολογίας του ΕΚΠΑ κ. Αλέξη Κελέκη, τους Επίκουρους Καθηγητές Επεμβατικής Ακτινολογίας του ΕΚΠΑ κ. Σταυρό Σπηλιόπουλο και κ. Δημήτρη Φιλιπιάδη, καθώς επίσης και τους Επεμβατικούς Ακτινολόγους κ. Χρυσόστομο Κωνσταντό, κ. Κωνσταντίνο Παλιαλέξη και κ. Λάζαρο Ρέππα που μου έδωσαν την ευκαιρία να συνεργαστώ μαζί τους. Επίσης θα ήθελα να πω ένα ευχαριστώ για την εξαιρετική συνεργασία στους τεχνολόγους- ακτινολόγους κ. Νίκη Παρμενίδου και κ. Κυριακό Αγγελόπουλο, καθώς επίσης και στους καταπληκτικούς νοσηλευτές Δέσποινα Χατζοπούλου και Θεοδωρή Θεοδώροπουλο και την γραμματέα Μαρία Λεβαντάκη. Ακόμα, ένα μεγάλο ευχαριστώ σε όλο το προσωπικό της Μονάδας Ακτινοφυσικής του Β΄ εργαστηρίου Ακτινολογίας, της Ιατρικής Σχολής του ΕΚΠΑ. Επίσης, δε θα ήμουν εδώ σήμερα εάν δεν ήταν η οικογένειά μου, που με έχει στηρίξει σε όλες μου τις επιλογές και την ευχαριστώ για ό,τι έχει κάνει για μένα. Τέλος, ένα μεγάλο ευχαριστώ στους φίλους μου για όλη την στήριξη και ιδιαίτερως στην Μαρία Κουτσοκάλη και τον Αλέξανδρο Ενό για τις πολύτιμες συμβουλές τους.

ΠΕΡΙΛΗΨΗ

Η πολυπλοκότητα των επεμβατικών διαδικασιών καθώς και οι υψηλοί ρυθμοί δόσης σε συνδυασμό με τη ραγδαία αύξηση των επεμβατικών πράξεων έχει σαν αποτέλεσμα τη σημαντική ακτινική επιβάρυνση των επεμβατικών ιατρών. Στόχος της παρούσας διπλωματικής εργασίας ήταν η αξιολόγηση των δόσεων ακτινοβολίας στους επεμβατικούς ακτινολόγους, στους φακούς των οφθαλμών και στο κεφάλι.

Για τις μετρήσεις χρησιμοποιήθηκαν δοσίμετρα θερμοφωταύγειας (TLDs) σε τρεις τύπους επεμβατικών πράξεων. Οι επεμβάσεις που μελετήθηκαν ήταν: **i)** 70 Αγγειοπλαστικές κάτω άκρων, **ii)** 15 Εμβολισμοί και Χημειοεμβολισμοί ήπατος και **iii)** 13 Σπονδυλοπλαστικές. Στη μελέτη συμμετείχαν δυο ομάδες επεμβατικών ακτινολόγων, εκ των οποίων η μία ομάδα διενεργούσε τις αγγειοπλαστικές κάτω άκρων και τους εμβολισμούς/ χημειοεμβολισμούς ήπατος, ενώ η άλλη τις σπονδυλοπλαστικές. Μια διάταξη των 7 δοσιμέτρων τοποθετήθηκε σε κάθε επεμβατικό ακτινολόγο, για κάθε είδος επέμβασης. Οι θέσεις τοποθέτησης των δοσιμέτρων ήταν οι ακόλουθες: αριστερός κρόταφος, επάνω από το αριστερό φρύδι, επάνω από το δεξί φρύδι, δεξιός κρόταφος, κοντά στον αριστερό οφθαλμό, ανάμεσα στους οφθαλμούς και κοντά στον δεξιό οφθαλμό από όπου και εξήχθησαν οι αντίστοιχες τιμές δόσεων.

Διενεργήθηκαν στατιστικοί έλεγχοι για την πιθανή ύπαρξη διαφοράς ανάμεσα στις δόσεις ανά διαδικασία, από την αριστερή και δεξιά πλευρά του κεφαλιού καθώς επίσης και στις δόσεις ανά διαδικασία στο επίπεδο των φακών των οφθαλμών και του μετώπου. Επιπλέον, πραγματοποιήθηκε στατιστικός έλεγχος για την διερεύνηση συσχέτισης των χρόνων εμπειρίας των επεμβατικών ακτινολόγων και των δόσεων τους ανά διαδικασία. Επίσης, ελέγχθηκε η ύπαρξη γραμμικής σχέσης της δόσης ανά επιφάνεια (DAP) με τη δόση ανά διαδικασία των επεμβατικών ακτινολόγων, καθώς και της δόσης ανά διαδικασία των ανατομικών περιοχών της αριστερής και δεξιάς πλευράς του κεφαλιού. Τέλος, έγινε εκτίμηση των αποτελεσμάτων σε σχέση με τα προτεινόμενα ετησία όρια για τους επεμβατικούς ακτινολόγους.

Συμπερασματικά, ανάμεσα στα τρία είδη επεμβάσεων που μελετήθηκαν, οι σπονδυλοπλαστικές ήταν εκείνες που έδωσαν τα μεγαλύτερα επίπεδα ακτινικής επιβάρυνσης τόσο στη θέση του πρώτου επεμβατικού ακτινολόγου όσο και του δεύτερου. Τα αποτελέσματα των στατιστικών ελέγχων έδειξαν ότι: η αριστερή πλευρά του κεφαλιού λαμβάνει μεγαλύτερη δόση από την δεξιά όπως και οι φακοί των οφθαλμών σε σύγκριση με το μέτωπο. Η εμπειρία του ακτινολόγου φαίνεται να σχετίζεται με την δόση που θα λάβει στο φακό του αριστερού οφθαλμού, άλλα όχι για τις υπόλοιπες ανατομικές περιοχές που μελετήθηκαν. Το DAP και η δόση ανά διαδικασία δεν βρέθηκαν να παρουσιάζουν γραμμική εξάρτηση. Αντιθέτως ισχυρή γραμμική εξάρτηση φαίνεται να παρουσιάζουν οι ανατομικές περιοχές της αριστερής πλευράς του κεφαλιού με τις αντίστοιχες της δεξιάς. Τέλος, πρέπει να τονιστεί ότι η χρήση του ακτινοπροστατευτικού εξοπλισμού είναι επιβεβλημένη έτσι ώστε να μην υπερβαίνονται τα ετήσια επαγγελματικά όρια.

ABSTRACT

The complexity of interventional radiology procedures as well as the high dose rates in conjunction with the rapid increase of interventional radiology procedures, have led to increased exposure levels among interventional radiologists. The aim of this master thesis was the evaluation of the radiation dose to the eye lens and head of interventional radiologists.

The measurements were conducted with thermoluminescence detectors (TLDs) for three general types of interventional procedures, including: **i)** Angioplasties lower limbs (N=70), **ii)** Embolizations/Chemoembolizations (N=15) and **iii)** Vertebroplasties (N=13). Two groups of interventional radiologists participated in this study; the one group performed DSA/PTA LL and Embolization/Chemoembolization procedures and the other Vertebroplasty procedures. A set of 7 dosimeters was attached to each physician for each procedure. TLDs' positions were the following: left side of the temple, over the left eyebrow, over the right eyebrow, right side of the temple, near the left eye, in the middle of the eyes and near the right eye from which the corresponding doses were calculated.

Statistical tests were performed for detecting possible differences between the doses per procedure on the left and right sides of the head, as well as between the doses per procedure to the eye lenses and forehead. In addition, statistical tests were used to demonstrate whether there was a correlation between the interventional radiologists' experience and the received doses per procedure. Furthermore, we examined whether there was a linear relationship between the DAP and the dose per procedure, as well as between the doses per procedure on the head's left and right side. In the end, we compared the results with the recommended occupational annual limits.

In conclusion, among the three types of procedures examined Vertebroplasties deliver the highest values of radiation burden both to the primary and assistant operator. The statistical tests' results revealed that the left side of the head received higher dose than the right, as well as the eye lenses than the forehead. Moreover, the interventional radiologist's experience correlated only with the received dose on the left eye lens. The results showed there is no linear relationship between the DAP and the doses in any of the examined anatomic regions. On the other hand, a strong linear relationship was found between the doses per procedure on the head's left and right side. Finally, we should emphasize that the use of radiation protective devices is of critical importance in order to avoid exceeding of the occupational annual limits.

Table of contents

ΠΡΟΛΟΓΟΣ.....	II
ΕΥΧΑΡΙΣΤΙΕΣ.....	II
ΠΕΡΙΛΗΨΗ.....	III
ABSTRACT.....	IV
TABLE OF CONTENTS.....	V
1 INTRODUCTION.....	1
1.1 BACKGROUND.....	1
1.2 AIM.....	1
2 THEORETICAL OVERVIEW.....	2
2.1 DOSE QUANTITIES.....	2
2.1.1 Absorbed dose.....	2
2.1.2 Equivalent dose.....	2
2.1.3 Effective dose.....	3
2.1.4 Dose area product.....	4
2.2 HARMFUL EFFECTS OF IONIZING RADIATION.....	5
2.2.1 Stochastic effects.....	5
2.2.2 Deterministic effects.....	5
2.2.2.1 Skin injuries.....	6
2.2.2.2 Cataract formation.....	7
2.2.2.3 Brain diseases.....	8
2.3 C-ARM FLUOROSCOPY UNIT.....	9
2.3.1 Basic components.....	10
2.3.1.1 The X-ray tube.....	10
2.3.1.2 Beam filtration.....	11
2.3.1.3 Collimation.....	11
2.3.1.4 Patient's table.....	11
2.3.1.5 Anti-scatter grid.....	12
2.3.1.6 The X-ray detector.....	12
2.3.1.7 Image display.....	13
2.3.2 Parameters affecting the radiation dose.....	13
2.3.2.1 C-ARM'S Angulation.....	13
2.3.2.2 Magnification.....	14
2.3.2.3 X-ray detector's distance from the patient.....	14
2.3.2.4 Time of exposure.....	15
2.3.2.5 Protective equipment.....	15
2.3.2.6 Patient's Body size.....	15
2.3.2.7 Interventional specialist's experience.....	16
2.3.2.8 Procedure's type.....	16

2.4	THERMOLUMINESCENCE DOSIMETER (TLD).....	17
2.4.1	<i>Thermoluminescence mechanism</i>	17
2.4.2	<i>TLD's Characteristics</i>	18
2.4.3	<i>Read-out and annealing process</i>	19
2.4.4	<i>TLDs' Calibration</i>	20
2.4.5	<i>Element correction coefficient</i>	21
2.5	INTERVENTIONAL RADIOLOGY PROCEDURES	22
2.5.1	<i>Angiography and angioplasty</i>	22
2.5.2	<i>Embolization/Chemoembolization</i>	22
2.5.3	<i>Vertebroplasty</i>	23
3	MATERIALS AND METHODS.....	24
3.1	PROTOCOL.....	24
3.2	INTERVENTIONAL RADIOLOGISTS' BEHAVIOR	25
3.3	TLDS MANAGEMENT	26
3.3.1	<i>Element correction coefficient (ECC)</i>	27
3.3.2	<i>TLDs annealing</i>	28
3.3.3	<i>TLDs read-out process</i>	28
3.3.4	<i>Calibration</i>	30
3.4	DATA ANALYSIS.....	33
4	RESULTS	34
4.1	INTERVENTIONAL RADIOLOGISTS' PROFILE	34
4.2	DSA/PTA LL PROCEDURES.....	35
4.3	EMBOLIZATION/CHEMOEMBOLIZATION PROCEDURES	36
4.4	VERTEBROPLASTY PROCEDURES	37
4.5	RADIATION DOSE FROM IR PROCEDURES.....	38
4.6	ESTIMATION OF THE ANNUAL DOSE	40
4.7	CORRELATION OF DAP-DOSE PER PROCEDURE.....	42
4.8	STATISTICAL ANALYSIS OF THE DOSES PER PROCEDURE FOR THE ANATOMIC REGIONS OF INTEREST	44
4.9	STATISTICAL ANALYSIS OF THE CORRELATION OF DOSES PER PROCEDURE AND THE OPERATOR'S EXPERIENCE.....	45
4.10	LINEAR RELATIONSHIP OF THE DOSE PER PROCEDURE ON THE EYES AND THE FOREHEAD.....	46
5	DISCUSSION.....	47
6	CONCLUSION	51
	REFERENCES.....	52

1 Introduction

1.1 Background

Interventional Radiology (IR) is a medical field associated with high occupational exposures. During the last decade a rapid increase has been observed in the number of interventional radiology procedures, due to the advantages offered by these minimally invasive techniques. As a result, interventional radiologists are chronically exposed to ionizing radiation which is associated with the development of eye lens opacities [1, 2] and increased risk of cancer. Recent studies have examined whether there is a link between ionizing radiation and brain malignancies to interventional radiologists and cardiologists [3, 4]. Additionally, many research papers recommended a reduction of the annual dose limit to the eye lens for occupational exposure, and the reduction of the threshold for radiation-induced cataract. Both proposals have already been adopted by the International Commission on Radiological Protection (ICRP). Therefore, the new annual dose limit is 20 mSv/year, when the previous dose limit was 150 mSv/year and the new threshold for cataract formation is 0.5 Gy [5].

Nonetheless, some investigators express the view that cataract may be a stochastic phenomenon [2]. According to literature, so far there is no clear connection between brain tumors (e.g. glioblastoma) and interventional radiology, since the interventional radiologists/cardiologists' sample participated in the studies is limited [4]. For these reasons, there is a need for more systematic monitoring of the doses to the anatomic regions, which are not protected by the lead-apron. Such regions are: the eye lenses, head and extremities, which can receive high doses when there is intensive workload and non-usage of protective equipment (e.g. lead glasses, ceiling suspended shield, table shield, lead gloves, etc.).

1.2 Aim

The purpose of this study was to measure and evaluate the radiation dose to the eye lens and head of interventional radiologists at the General University Hospital Attikon, in three general categories of interventional radiology procedures: **i)** Angiographies and angioplasties Lower Limb (DSA- Digital Subtraction Angiography/PTA-Percutaneous Transluminal Angioplasty LL-Lower Limb), **ii)** Embolization/Chemoembolization procedures and **iii)** Vertebroplasty procedures. The measurements were performed with thermoluminescent dosimeters (TLDs) consist of Lithium Fluoride and impurities of Magnesium and Titanium (*LiF:Mg,Ti*). Also, the occupational radiation doses were correlated with parameters such as: DAP, type of procedure, physician's experience, the distance of the flat panel from the patient, and the use of protective equipment.

2 Theoretical overview

2.1 Dose Quantities

In the current unit, the basic dosimetric quantities are presented.

2.1.1 Absorbed dose

The absorbed dose, D , is the quotient of $d\bar{\epsilon}$ by dm , where $d\bar{\epsilon}$ is the mean energy imparted by ionizing radiation to matter of mass dm , thus D :

$$D = \frac{d\bar{\epsilon}}{dm}$$

In other words, the non-stochastic quantity absorbed dose is defined as the statistical average of the energy imparted per unit mass at a point. The unit for radiation absorbed dose in the SI system is the *gray* (Gy) and is defined as follows:

$$1\text{Gy} = \frac{1\text{J}}{1\text{kg}}$$

One *gray* is an absorbed radiation dose of one joule per kilogram.

The gray unit is universally applicable to all types of ionizing radiation dosimetry due to external fields of gamma rays, neutrons, or charged particles as well as internally deposited radionuclides.

2.1.2 Equivalent dose

The absorbed dose is not a reliable indicator of the possible biological effects. As a reference, 1 Gy of alpha radiation would be much more biologically damaging than 1 Gy of photon radiation. Therefore, appropriate weighting factors can be applied reflecting the different relative biological effects for each radiation type. For this reason, a protection quantity was defined, which is known as equivalent dose (H_T). The equivalent dose, H_T , is defined by

$$H_T = \sum_R W_R \cdot D_{T,R}$$

Where $D_{T,R}$ is the mean absorbed dose in a tissue T due to radiation of type R and W_R the corresponding radiation weighting factor (see: **Table 2.1.1**, **Fig. 2.1.1**). The sum is calculated for all types of radiation involved. The unit of radiation weighted dose is J per Kg and has the special name Sievert (Sv).

Table 2.1.1 Radiation weighting factors [6]

Radiation type	Radiation weighting factors, W_R
Photons	1
Electrons and muons	1
Protons and charged pions	2
Alpha particles, fission fragments, heavy ions	20
Neutrons	See Fig. 2.1

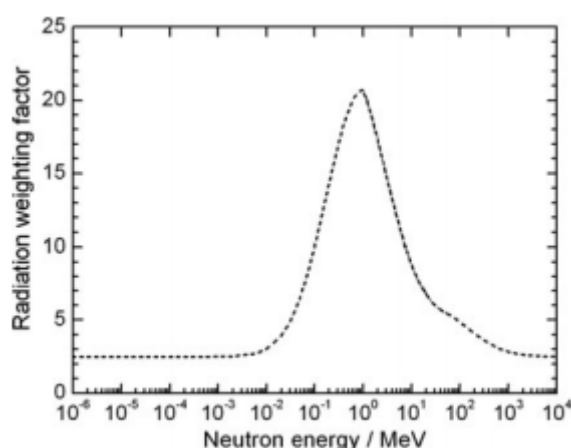


Fig. 2.1.1 Radiation weighting factor, W_R , for neutrons versus neutron energy [6]

2.1.3 Effective dose

The effective dose is used to compare the stochastic risk of non-uniform exposure to radiation. Each body tissue reacts differently to each type of radiation and cancer-induction occurs at different dose rate to different tissues. Hence, the effective dose is the risk of developing fatal cancer in the tissue. If the body is uniformly irradiated, the summed effective doses are equal to 1. The effective dose, E , is defined by a weighted sum of tissue equivalent doses as:

$$E = \sum_T W_T \cdot H_T = \sum_T W_T \cdot \sum_R W_R \cdot D_{R,T}$$

Where W_T is the tissue weighting factor for tissue T and $\sum W_T = 1$. The sum is calculated for all organs and tissues of the human body, considered to be sensitive to the induction of stochastic effects. These W_T values (see: **Table 2.1.2**) are chosen to represent the contributions of individual organs and tissues to overall radiation detriment from stochastic effects. The unit of effective dose is Sievert (Sv) (J per kg).

Table 2.1.2 Recommended tissue weighting factors [6]

Tissue	W_T	$\sum W_T$
Bone-marrow (red), Colon, Lung, Stomach, Breast, Remainder tissues*	0.12	0.72
Gonads	0.08	0.08
Bladder, Oesophagus, Liver, Thyroid	0.04	0.16
Bone surface, Brain, Salivary glands, Skin	0.01	0.04
TOTAL	-	1.00

* Remainder tissues: Adrenals, Extrathoracic region, Gall bladder, Heart, Kidneys, Lymphatic nodes, Muscle, Oral mucosa, Pancreas, Prostate, Small intestine, Spleen, Thymus, Uterus/cervix.

2.1.4 Dose area product

Dose area product (DAP) is a product of the surface area of the patient that is exposed to radiation through the skin entrance, in square centimeters or square meters, multiplied by the radiation dose of this surface in grays. DAP is valuable because radiation-induced bioeffects are directly related to both the radiation dose and the total amount of tissue that is irradiated. Moreover, many new fluoroscopy and angiography units include a special ionization chamber at the surface of the x-ray tube collimator that measures DAP, making these values directly available. DAP is a better risk indicator than entrance dose. DAP has been shown to correlate well with the total energy imparted to the patient, which is related to the effective dose and therefore to the overall cancer risk.

2.2 Harmful effects of ionizing radiation

As it is widely accepted, ionizing radiation could induce chemical changes in cells and damage them. Some cells may lead to apoptosis, necrosis or genetic variation. The effects, that have been associated with ionizing radiation, are classified to deterministic and stochastic effects (see: Fig. 2.2.1). Stochastic effects occur by chance, usually without a threshold. On the other hand, deterministic health effects increase in severity with the increasing of the dose above a threshold.

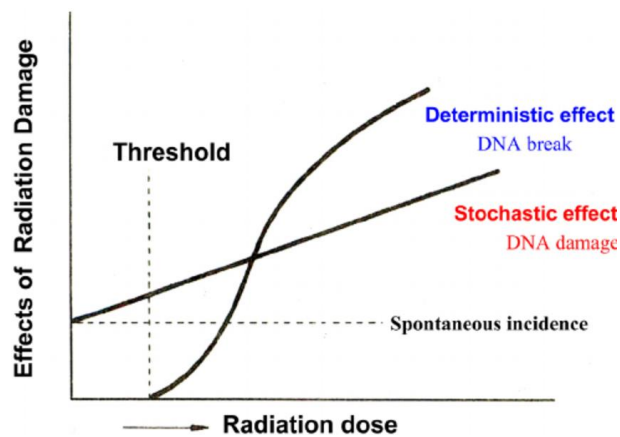


Fig. 2.2.1 Classification of radiation effects. [7]

2.2.1 Stochastic effects

Stochastic effects are those effects that occur by chance, with the probability of the effect increasing with dose, but the severity of the effect is independent of the dose received. For stochastic effects, there is no threshold dose below which it is certain that an adverse effect cannot occur. In addition, because stochastic effects can occur in individuals that have not been exposed to radiation above background levels, it can never be determined for certain that cancer incidence or genetic damage was due to a specific exposure. The International Commission on Radiological Protection indicates a value of 5.5 % per Sievert for cancer and 0.2 % per Sievert for heritable effects after exposure to radiation at low dose rate [6].

2.2.2 Deterministic effects

In contrast to stochastic effects, deterministic effects only occur when a threshold from exposure has been exceeded, where the threshold level is different for each organ or tissue. Also, deterministic effects increase in severity and incidence with dose. Thus, in some cases, the sensitivity of the method of detection is fundamental. For example, clinical methods are available to detect small radiation-induced lesions in the lens of the eye which do not affect vision significantly. The time at which deterministic effects can be detected after irradiation varies among tissues, which are classified as

early-responding and late-responding. Some other examples of ionizing radiation deterministic effects are: skin injuries and non-cancer brain diseases.

2.2.2.1 Skin injuries

As it is well known, ionizing radiation can cause skin reactions and injuries. Skin injuries occur for doses higher than a threshold and depend on the dose received by the skin. The effects are distinguished in prompt (< 2 weeks), early (2-8 weeks), midterm (6-52 weeks) and long-term (>40 weeks) [8]. Tissue reactions in relation to absorbed dose are presented in **Table 2.2.1**. One example of procedures that can provoke skin injuries are interventional radiology procedures. These procedures may deliver a high skin entrance dose, and in rare occasions, some of them may cause serious skin injuries. Therefore, monitoring radiation dose is essential. The display of radiation dose indicators are required by the U.S. Food and Drug Administration's regulations and by the International Electrotechnical Commission's standards [9, 10]. These displays usually include the reference point of air kerma (kinetic energy released per unit mass) and DAP. When the reference point of air kerma is used appropriately, it provides a useful clinical indicator to radiologist of the likelihood of skin injury. Also DAP is used to estimate the risk of a stochastic effect (e.g., cancer) [11].

Table 2.2.1 Tissue Reactions from Single-Delivery Radiation Dose to Skin of the Neck, Torso, Pelvis, Buttocks, or Arms [11].

Band	Dose ^a (Gy)	National Cancer Institute Grade	Approximate Time of Onset of Effects			
			Prompt (<2 wk)	Early (2–8 wk)	Midterm (6–52 wk)	Long Term (> 40 wk)
A1	0–2	NA	No observable effects expected	No observable effects expected	No observable effects expected	No observable effects expected
A2	2–5	1	Transient erythema	Epilation	Recovery from hair loss	No observable effects expected
B	5–10	1	Transient erythema	Erythema and epilation	Recovery; after higher doses, prolonged erythema and permanent partial epilation expected	Recovery; after higher doses, dermal atrophy and induration expected
C	10–15	1–2	Transient erythema	Erythema and epilation; possible dry or moist desquamation; recovery from desquamation	Prolonged erythema; permanent epilation	Telangiectasia ^b ; dermal atrophy and induration; skin expected to be weak
D	> 15	3–4	Transient erythema; after very high doses, edema and acute ulceration expected, with surgical intervention most likely required in longer term	Erythema and epilation; moist desquamation	Dermal atrophy; secondary ulceration due to failure of moist desquamation to heal, with surgical intervention most likely required	Possible late skin breakdown; wound might persist and progress to a deeper lesion, with surgical intervention most likely required

2.2.2.2 Cataract formation

Cataract is an ocular lens opacity of the eye, associated with visual impairment and may be classified according to, anatomic location to three main forms:

- i) nuclear,
- ii) posterior subcapsular (PSC) and
- iii) cortical or mixed types.

Nuclear refers to the central portion of the lens, called the nucleus. Cortical refers to the lens cortex, which is the peripheral (outside) edge of the lens. Posterior subcapsular refers to the posterior, which is the back surface of the lens and "subcapsular" as it is beneath the lens capsule, which is a small "sac", or membrane, that encloses the lens and holds it in place.

The lens of the eye is sensitivity to ionizing radiation and cataract formation has been recognized as a major ocular complication, associated with the exposure to ionizing radiation [12, 13]. Among the three main forms of cataract, studies have shown that posterior subcapsular and cortical cataract are associated with exposure to radiation [14]. Cataractogenic radiation damage occurs at the "germinative zones" at the anterior surface, where dividing cells form a clear crystalline-protein fiber that migrates towards the posterior pole of the lens, the posterior subcapsular region. Radiation damage by both direct and oxidative mechanisms causes DNA breaks, aberrant cell migration and complex biochemical alterations that result in aberrant crystalline protein folding and dysregulation of lens cell morphology [15].

Historically, PSC was thought to be the predominant lesion of radiation damage to the lens, although more recent data suggest that radiation induced opacities can be found in the lens cortex as well. The latency period between irradiation and cataract formation is inversely proportional to dose and it ranges from years to decades [2, 16]. The new threshold for cataract formation is 0.5 Gy and the occupational annual dose limit is 20 mSv, averaged over defined periods of 5 years, with no single year exceeding 50 mSv [5]. The previous annual dose limit for the eye lens was 150 mSv, in terms of equivalent dose and the previous threshold for detectable lens opacities, was considered to be 5 Sv for chronic exposure, 0.5-2.0 Sv for acute exposure, 8 Sv for fractional exposure and 5 Sv for acute exposure for visual impairment (cataract) [17]. Nonetheless, some investigators express the view that cataract is a stochastic phenomenon [2, 18]. These changes were adopted when several studies raised concerns about the annual dose limit to the eye lens, for occupational exposure, and the threshold for radiation-induced cataract, recommending the reduction for them both [2, 14, 18, 19].

One of the health professionals, who are at risk of radiation induced eye lens injury, is interventional radiologists [16]. Interventional radiologists are usually within a high-scatter X radiation field for several hours a day, during IR procedures. The risk for eye lens injuries is particularly high for intense workloads, unless the appropriate protective devices (either personal or catheterization's laboratory protective devices) and proper operational techniques are applied.

2.2.2.3 Brain diseases

According to the fundamental law of radiology, Bergonie and Tribodeau (1906), “the sensitivity of cells to irradiation is direct proportion to their reproductive activity and inversely proportional to their degree of differentiation”. Therefore, the brain is a great example of a highly differentiated organ with low mitotic activity, and as a consequence, it is radio-resistant.

However, ionizing radiation has been established as one of the causes of brain cancer. In particular, among the interventional cardiologists/radiologists, there are evidences for a link between ionizing radiation and brain malignancies. The dose to the left side of the head to these specialists is, in most cases, greater than the right [20]. This is because, they usually work on the patient’s right side, so their left side is closer to the x-ray tube. In most of the cases recorded, the brain malignancies of the interventional physicians were located on the left side [4, 21]. Nevertheless, there is not a clear connection, due to limited sample size [4, 21, 22]. Additionally, ionizing radiation may provoke non-cancer effects, too. Several epidemiological and cardiovascular-diseases studies, concluded that there is a significant association between radiation exposure and circulatory disease, either cardiovascular or cerebrovascular [3]. Radiation may induce atherosclerosis in large vessels [23], which resulted in the increase of cardiovascular disease and stroke risk [24].

Brain is an organ where the mitotic activity is reduced or null. However, hippocampus and olfactory is two structures, that neurogenesis continues after birth. Thus, these structures are sensitive to radiation [3, 25]. Hippocampus is important for memory and other brain functions. Studies have indicated that radiation-induced arrest of neurogenesis, to hippocampus and olfactory bulb, may lead to neurocognitive disorders [3, 25].

2.3 C-ARM Fluoroscopy Unit

Fluoroscopy is a real time imaging technique, which is used to visualize internal structures of human body for assisting to medical professionals in surgical procedures. Early fluoroscopy systems consisted simply of an X-ray source and a fluorescent screen, and the patient was situated between them. After passing through the patient, the photon beam impacted the fluorescent screen and produced a visible glow, which was directly observed by the physician. The modern fluoroscopy systems are more complicated. The fluorescent screen is coupled with an electronic device that amplifies and transforms the glowing light into a video signal suitable for presentation on an electronic display. Therefore, the dose to the physician and the patient has been radically decreased. These systems are called C-ARM and the name derives from the C-shaped arm used to connect the x-ray source and x-ray detector to one another (see: **Fig. 2.3.1**).

The key components of C-ARM fluoroscopic unit are: an X-ray tube, spectral shaping filters, a field restriction device (collimator), an anti-scatter grid, an X-ray detector (flat panel or image intensifier), a display device (monitor), a patient-support device (table or couch) and a high-voltage generator. Additionally, it is essential to mention, that the use of radioprotection equipment is mandatory during fluoroscopically guided procedures. The main radioprotection devices are: ceiling suspended shield, table shield, individual lead apron, lead glasses and lead gloves.

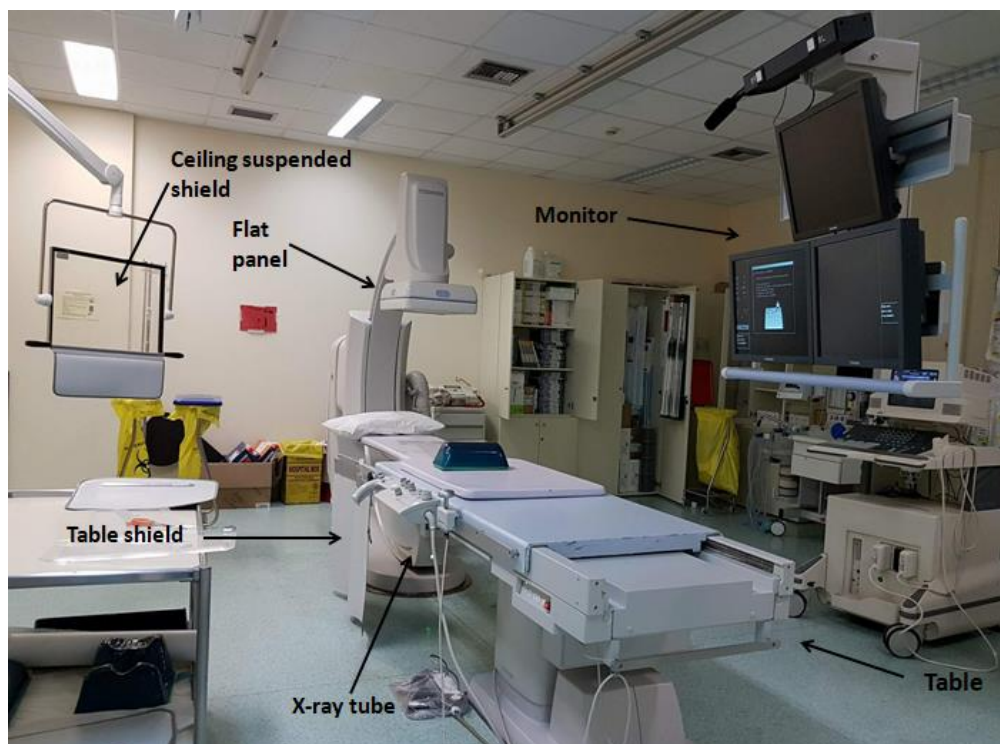


Fig. 2.3.1 C-ARM fluoroscopy unit with its components

2.3.1 Basic components

2.3.1.1 The X-ray tube

An x-ray tube is a vacuum tube that converts electrical input power into x-rays (see: **Fig. 2.3.2**). The quantity (exposure) and quality (spectrum) of the x-radiation produced can be controlled by adjusting the electrical quantities (kV – voltage or the potential applied to the tube, mA – current that flows through the tube) and the tube's exposure time. The energy used by the x-ray tube to produce x-ray radiation is supplied by a high voltage generator. The main feature of the generator is to amplify the electrical energy from the electrical power systems and convert the alternating current (AC) into the direct current (DC).

The x-ray production is based on a process known as thermionic emission. A small coil of wire (a filament) is heated and expels the electrons (cathode). After the electrons are emitted from the cathode, they come under the influence of an electrical force pulling them toward a target (anode). The anode is usually made from tungsten. When the electrons impact the anode, their kinetic energy converts into: x-radiation and heat. The 99% of the electrons' kinetic energy turn into heat and only 1% change to x-rays. For this reason, the anode is rotated, in order to dissipate the heat.

The radiation is produced within a very small area on the anode's surface known as the focal spot. The dimensions of the focal spot are determined by the dimensions of the electron beam reaching from the cathode and usually range from 0.1 mm to 2 mm. The x-ray tubes are designed to have specific focal spot sizes. Small focal spots produce less blurring and more detailed visibility, whereas large focal spots have a greater heat-dissipating capacity. The produced x-rays rely on the bremsstrahlung effect.

In addition, in the case of electrons, with high enough energy to expel an electron out of the atomic shell of the anode's bombarded atoms, characteristic x-rays are produced.

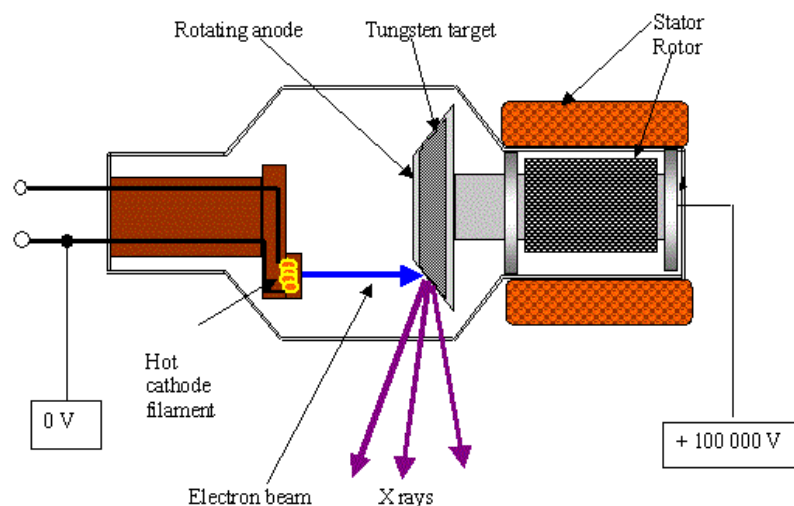


Fig. 2.3.2 View of an X-ray Tube

2.3.1.2 Beam filtration

The X-ray beam that emerges from the tube has a continuous spectrum of photons with characteristic x-ray peaks (see: **Fig. 2.3.3**). Only a few of the emitted photons have energy close to the energy of the electrons that produced them. Most of the photons produced have lower energy. These lower energy photons are absorbed by the patient and they do not impact to the establishment of the medical image. In that case, the patient's dose will be increased. In order to eliminate the low energy photons, without affecting the high energy photons, an appropriate filter is used. The filter is located at the x-ray's tube exit and the filter is usually made of aluminum or copper. One more advantage of the beam filtration's use is the increase of the medical image's contrast.

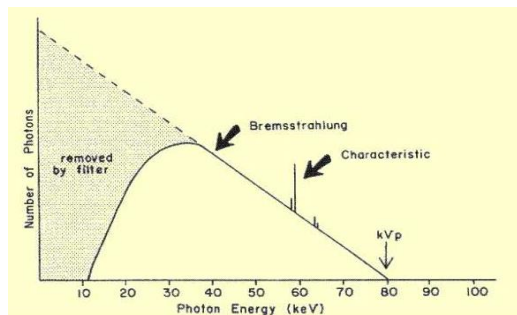


Fig. 2.3.3 Typical spectrum from x-ray tube at 80 Kv

2.3.1.3 Collimation

Collimators are pairs of lead shutters that limit the geometric extent of the X-ray field which occurs in all X-ray equipment. In this way, the dose to the patient and the medical staff is reduced. Moreover, the quality of medical image is improved, as a result of the decrease scatter radiation from patient, which provokes low contrast. In fluoroscopy, the collimation may have a circular or rectangular shape, matching the shape of the x-ray detector.

2.3.1.4 Patient's table

The patient's table must be durable to support patients, so they are classified, by the manufacturer, for a particular weight limits. It is important that the table not absorb much radiation, in order to avoid shadows, loss of signal and loss of contrast in the image. Also, the table must have the ability to move to all directions (x, y, z) in assistance of the interventional radiologist. The carbon fiber technology offers a good combination of durability and minimal radiation absorption, making it an ideal table material. In addition, foam pads are often placed between the patient and the table for more comfort, yet with minimal radiation absorption.

2.3.1.5 Anti-scatter grid

Anti-scatter grids are standard components of fluoroscopic systems, since a large percentage of fluoroscopic examinations are performed in high-scatter conditions, such as in the abdominal region. The anti-scatter grid lessens the scattered photons, which are accountable for the degradation of medical image. Typical grid ratios range from 6:1 to 10:1. The grids may be circular (image intensifier systems) or rectangular (flat panel detector systems).

2.3.1.6 The X-ray detector

The x-ray detectors, of current fluoroscopy systems, are divided in two categories: the image intensifier and the flat-panel detectors (see: **Fig. 2.3.4**). The most conventional and older system is the image intensifier detector, which is coupled with a television camera system and displays. The image intensifier is a large vacuum tube, that captures the transmitted pattern of x-ray radiation from the patient and converts it into a light image of sufficient brightness, which is displayed on the television camera. After the x-rays enter the curved input surface of the image intensifier, they interact with a layer of phosphor, which is usually composed of cesium iodide, and deposit energy to it. The light from the phosphor layer is absorbed by the photocathode layer of the image intensifier, which uses the energy to emit electrons. A high voltage (25,000-35,000 V), which is placed between the input photocathode and the output phosphor layer of the image intensifier, accelerate the electrons. The high voltage is applied by electrostatic plates, which are used to focus and direct the electrons to the output phosphor. Subsequently, the electrons' kinetic energy is converted to light image. After passing through a lens system and an aperture, the television camera tube intercepts this light image and converts the light pattern into a series of electrical signals, that may be displayed on the television monitor.

In the recent years, the image intensifier detector and television camera components have been replaced by flat-panel detectors, which consist of an array of individual detector elements. Their typical size ranges from 140 μm to about 200 μm per side, depending on the manufacturer and model. The entire size of the flat-panel ranges from 25x25 cm^2 to 40x40 cm^2 . Due to the detector's elements sensitivity to light, a scintillation layer is appropriated. This layer, which is mostly composed of thallium-activated cesium iodide, attenuates the incident x-rays and produces light. The scintillation layer is composed of many needle-like crystals, which are grouped together to cover the surface of the detector element. These needle-like structures help direct light toward the photodiode, located below. When light hits the surface of the low-noise photodiode and transistor, placed below, it acts like a switch, allowing the diode to conduct electricity and an electronic signal is produced. In this way, each detector element is read in the flat-panel array row by row and an electronic image will be formed.

The flat-panel systems have multiple advantages, such as smaller size, extended dynamic range, no spatial distortion and greater stability. However, flat-panel systems typically have the same spatial resolution for all fields of view and are prone to ghosting.

The image intensifier systems have better spatial resolution, with the use of smaller fields of view (magnification modes), and tend to be less expensive. However, the spatial resolution of image intensifier systems is limited by the television camera system to which they are coupled. Moreover, image intensifier systems are degraded by glare, vignetting, spatial distortions, and defocusing effects, whereas the flat-panel systems do not have these problems.

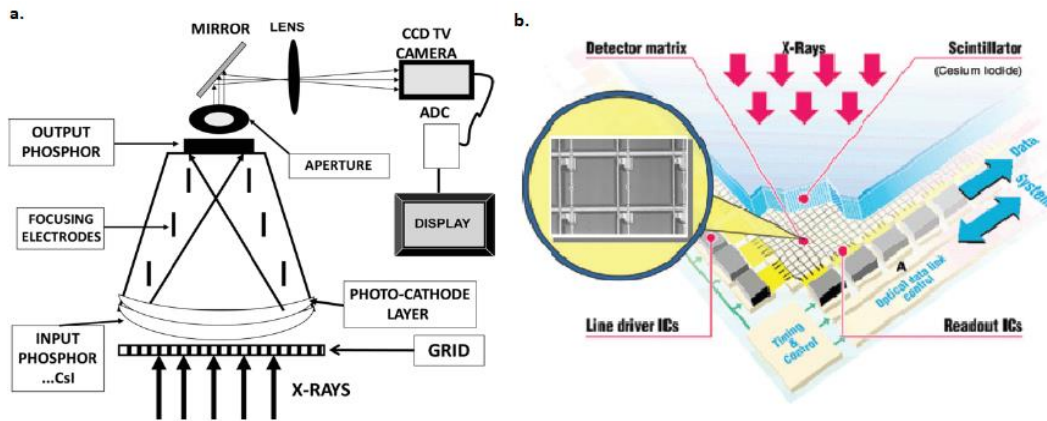


Fig. 2.3.4 (a) The internal structures of an image intensifier, (b) a section of the flat-panel detector and many individual detector elements.

2.3.1.7 Image display

Fluoroscopy requires high-quality video displays that allow users to appreciate fine details and subtle contrast differences, in the anatomic region of interest. The medical image display technology has relied on breakthrough technologies of the television industry over the last several years. Modern systems feature high resolution flat-panel LCDs with high maximum luminance and high-contrast ratios. These displays should be calibrated to a standard luminance response function, to ensure that the widest ranges of gray levels are visible.

2.3.2 Parameters affecting the radiation dose

During fluoroscopically guided procedures there are several parameters that affect the scatter radiation dose to the interventional radiologists/cardiologist, such as: the angulation of the C-ARM, the use of magnification, the distance of the x-ray detector from the patient, the time of exposure, the use of protective equipment, the body size of the patient, the physician's experience and the type of procedure.

2.3.2.1 C-ARM'S Angulation

Lateral projections, increase the scatter radiation dose to the physician [26, 27]. Whenever a projection with high obliquity is used, the photons have to pass through a thicker section of the patient's body. This, results in an increase of the fluoroscopic exposure parameters (mainly kV), in order to maintain image quality. According to

C.Koukorova et al. [27], the highest dose rate is measured at the Left Anterior Oblique 90° (LAO 90) projection, which corresponds to the lateral projection, when the operator is standing at the tube's side. Generally, when the C-arm angulation is above 30° the dose levels are significantly higher (see: **Fig. 2.3.5**).

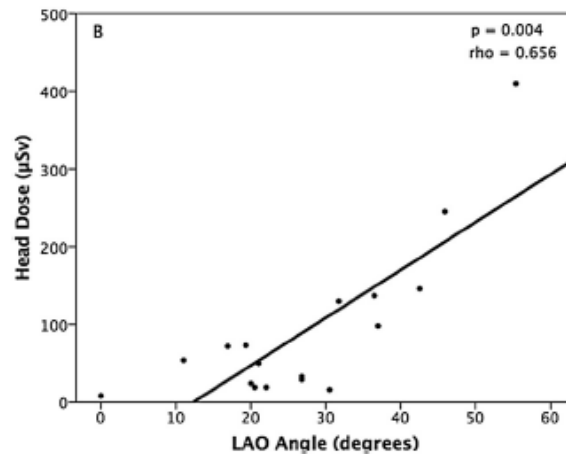


Fig. 2.3.5 The Scatter graph demonstrates the relation between LAO angle and head dose to primary interventional radiologist during Digital Subtraction Angiography (DSA). [28]

2.3.2.2 Magnification

The use of magnification during interventional procedures improves the spatial resolution of the image, which is sometimes necessary for accurate diagnosis and therapy. However, the radiologist/cardiologist should use the magnification with sense, as it is a parameter that directly affects the radiation dose to the patient and the medical staff.

2.3.2.3 X-ray detector's distance from the patient

Another parameter, that influences the dose to interventional radiologist/cardiologist, is the distance between the x-ray detector and the patient. The optimal distance between the patient and the x-ray detector surface, must be as much closer to the patient as possible. This technique decreases the dose received by the physician, due to the reduction of the scatter radiation. Furthermore, one more parameter that should be considered is the source-to-patient distance. If the patient is close to the x-ray tube, there is more exposure to him/her via the inverse square law. Therefore, the optimal technique is for the distance between the patient and the x-ray detector to be as small as possible, whereas the distance between the patient and the x-ray source to be as long as possible, so the interventional radiologist and the patient will be protected by ionizing radiation (see: **Fig. 2.3.6**).

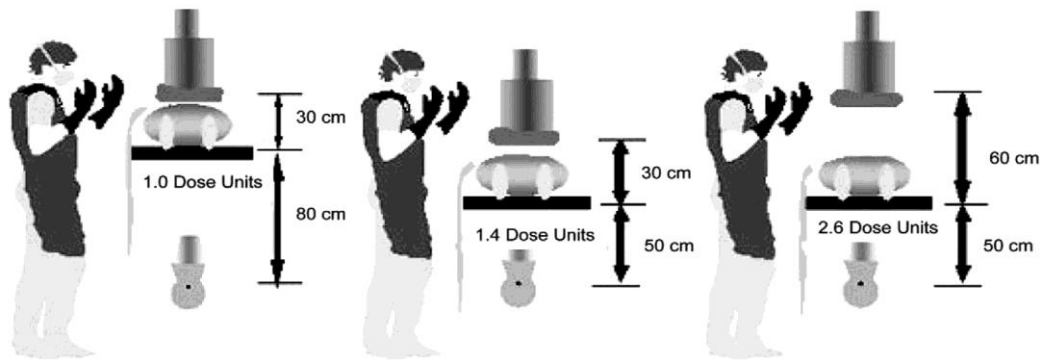


Fig. 2.3.6 The effects of various relationships between the patient, x-ray and x-ray detector distance. The optimal technique is shown in the first figure.

2.3.2.4 Time of exposure

The time of the interventional radiologist exposure, while performing a procedure, is related to the scatter dose. The longest time needed for the procedure, the longest the physician's exposure to radiation. Usually, the most extended procedures, result to higher levels of scattering radiation exposure [28].

2.3.2.5 Protective equipment

During interventional procedures, the patient's scattered radiation is the main source of radiation dose received by the medical staff. The radiation dose can be reduced by using personal protective devices (e.g. lead apron, lead glasses, thyroid collar, protective cap, lead gloves etc.) along with catheterization laboratory protective devices (e.g. lead shielding ceiling, table lead curtain and mobile floor screen). According to the lead aprons' and lead shielding ceiling's manufacturers, each of them can attenuate the received scatter dose more than 90%, depending on the energy of the X-rays (kV setting) and the lead equivalent thickness of the protective device [29].

Nonetheless, professionals involved in fluoroscopy procedures should receive special training regarding radiation protection issues. Training should be targeted to the specific needs of fluoroscopy work, such as the right use of radioprotection devices, and it should be provided by an expert in radiation protection, such as a medical physicist.

2.3.2.6 Patient's Body size

In X-ray imaging, occupational radiation risk arises mainly from the scattering of X-rays impinging on the patient. The patient's body size is the dominant parameter that affect the scatter dose. Patient's body thickness determines the kV and mA that should be used. The automatic control system (AEC) will select higher exposure quantities for thicker patients and thus the medical staff will be exposed to higher scattered radiation [30, 31]. According to E. Vano et al.[30], on fluoroscopy and cine modes, as the patient's thickness increases, the occupational doses can increase up to 30 times than the baseline level.

2.3.2.7 *Interventional specialist's experience*

The physician's experience is a parameter, which may affect the dose. Usually, an experienced interventional radiologist/cardiologist can complete a procedure in a shorter period of time comparing to a younger and less experienced specialist. Therefore, the most experienced radiologists usually receive lower radiation dose.

2.3.2.8 *Procedure's type*

A parameter, which dramatically influences the dose to the physician, is the type of procedure. There are various procedures with dissimilar complexity. This means that the scatter radiation from the patient may be different in relation to the type of procedure. For instance, according to, J. Domienik et al. [32] the highest doses, received by the main operator, have been observed during DSA/PTA R and Embolisations. For other types of procedures (e.g. DSA/PTA C&C, DSA/PTA LL) the received doses are all below 0.080 mSv, while for the ERCPs the doses are much lower (below 0.025 mSv). Furthermore, depending on the procedure, the parts of the operator's body that receive the highest doses are the left finger (DSA/PTA R) and the left wrist (DSA/PTA R), which were 0.14 mSv and 0.12 mSv, respectively. The highest doses to the eyes were measured during embolisations, which were 0.085 mSv for left eye and 0.059 mSv for the region between the eyes (see: **Fig. 2.3.7**).

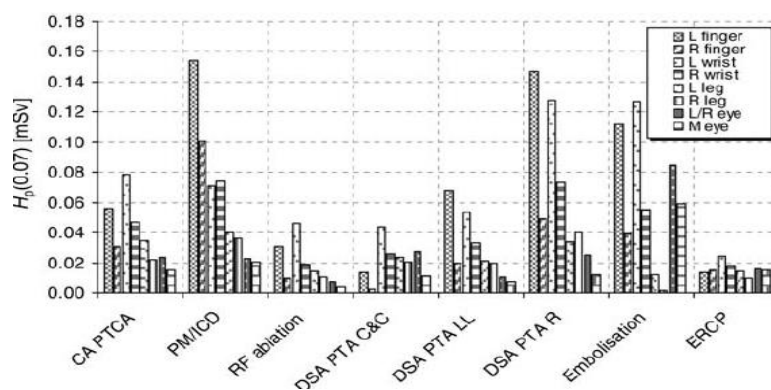


Fig. 2.3.7 The median dose to different parts of the body depending on the procedure [32]

2.4 Thermoluminescence dosimeter (TLD)

Radiation dosimeter is a device, instrument or system that measures or evaluate, either directly (active dosimeter) or indirectly (passive dosimeter), the quantities exposure, kerma, adsorbed dose or equivalent dose, or their rates, or related quantities of ionizing radiation. The dosimeter along with its reader is called as a dosimetry system. In order to function as a radiation dosimeter, the dosimeter must possess at least one physical property. For instance, the physical property of the thermoluminescence dosimeter (TLD) is the thermal activated phosphorescence (thermoluminescence) [33]. TLDs come in a variety of shapes and size (see: **Fig. 2.4.1**). They are the most popular dosimeters in the field of medical physics. Due to their multifunctionality, TLDs have found application in diagnostic radiology, radiation therapy, and health physics [34].

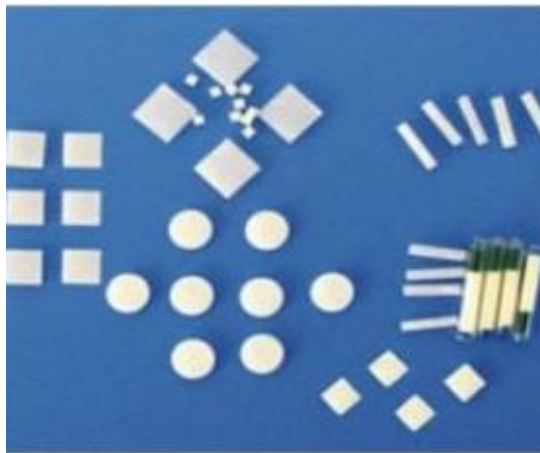


Fig. 2.4.1 Different shapes and sizes of TLDs

2.4.1 Thermoluminescence mechanism

The light emission from an irradiated material, through thermal process is well known as thermoluminescence. This phenomenon is present in many crystalline materials and is vital for the detection and quantification of ionizing radiation with TLDs [34].

According to, the band theory of solid the electrons are found in valence band. If electrons absorb energy greater than energy gap (E_g), when the material is irradiated, they move from the valence to the conduction band, where they move freely. Consequently, a hole is created in the valence band, where it can also move inside to crystal. Then, the free electrons and holes migrate into metastable states, which is known as electron and hole traps and they are located between the valence and the conduction band. These traps are energy wells and if the charge carriers have not enough energy, they cannot escape from them. By heating electrons and holes receive energy and then they release and recombine at luminescence centers (recombination centers). The recombination is characterized by release of visible light (see: **Fig. 2.4.2**).

It is important to mention that a pure thermoluminescence crystal does not show considerable luminescence. Therefore, the addition of trace amount of impurities in the

crystal lattice is essential, in order to boost the thermoluminescence properties. These added impurities in the crystal lattice create the trap centers and the luminescence centers. The probability (P) of a charge carrier to release from trap center, in reference of time is given by Randall-Wilkins theory as:

$$P = \frac{1}{\tau} = \alpha \cdot e^{-\frac{E}{kT}}$$

Where,

- τ = The mean half – life of a charge carrier in a trap
- α = The frequency factor
- E = The energy of the trap (eV)
- k = The Boltzmann's constant = $8.62 \cdot 10^{-5}$ eV/°K
- T = The Temperature (°K)

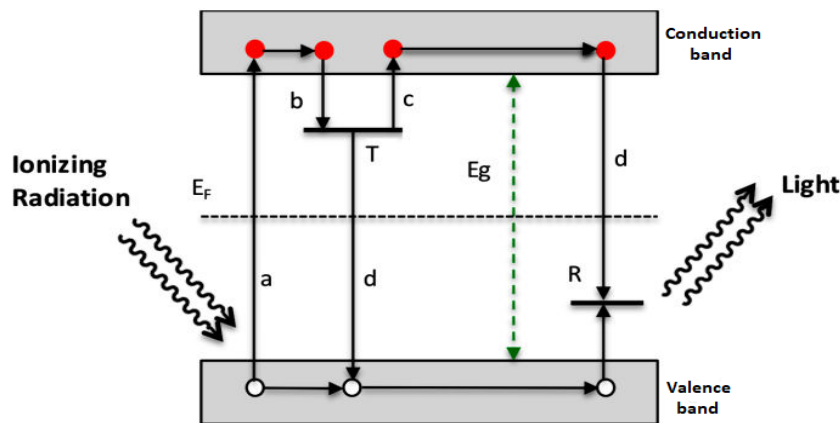


Fig. 2.4.2 Thermoluminescence process. (a) Irradiation and e^- moves to conduction band, (b) trapping, (c) de-trapping by thermal stimulation, (d) recombination [35].

2.4.2 TLD's Characteristics

Not all thermoluminescence materials are ideal for dosimetry. However, the TLDs have characteristics which make them suitable for measuring radiation dose. TLDs are very small, for this reason, they have a great extent to approach a point measurement. Also, their small size slightly disturbs the radiation field for medium to high-energy photon beams. Some of the TLDs used for determining the radiation dose, have low atomic number (Z) and are characterized as tissue-equivalent materials. These are: LiF: Mg, Ti, LiF: Mg, Cu, P and $\text{Li}_2\text{B}_4\text{O}_7$: Mn. They are used for medical applications as well as for personnel monitoring for industrial application [33, 34]. Two more characteristics of TLDs are accuracy and precision. The precision of dosimetry measurements specifies the reproducibility of the measurements under similar conditions and can be estimated from the data obtained in repeated measurements. High precision is associated with a small standard deviation of the distribution of the measurement results. The accuracy of dosimetry measurements is the proximity of their expectation value to the 'true value' of the measured quantity. The thermoluminescence signal decreases after irradiation due to

spontaneous emission of light at room temperature. This phenomenon is called fading. Typically, TLDs have low fading rate, which does not exceed a few per cent, in a period of months, after irradiation [33, 36].

Ideally, the signal from dosimeter reading should be in linear proportion to the received dose. However, beyond a certain dose range, a non-linearity is observed. TLDs present a wide range of linearity zone. When TLDs are not used in the linear region, a correction should be applied to the signal. Nevertheless, at high doses the supralinearity (or sublinearity) and saturation are unavoidable (see: **Fig. 2.4.3**) [36].

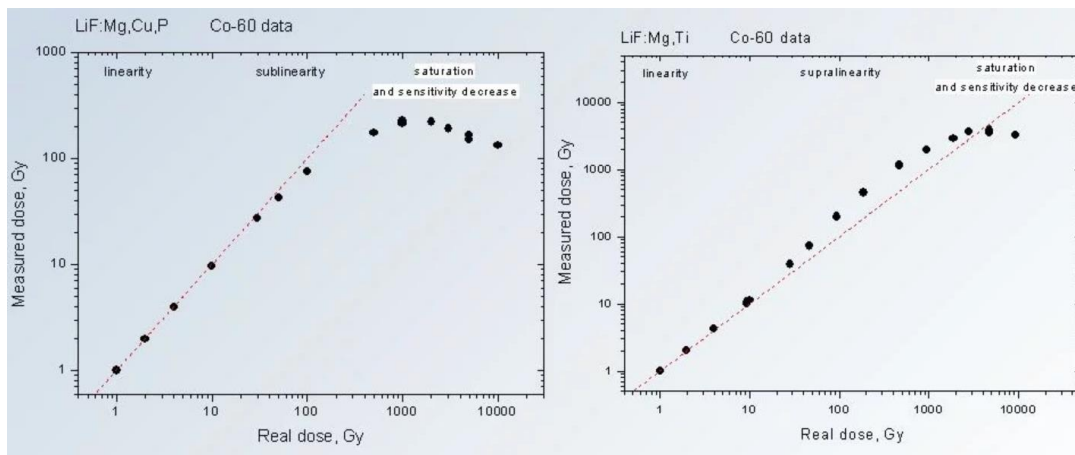


Fig. 2.4.3 Diagrams demonstrate linearity, sublinearity, supralinearity and saturation region of LiF:Mg, Cu, P (left diagram) and LiF:Mg, Ti(right diagram)

TLDs are characterized by adequate sensitivity. Sensitivity may be defined as the amount of light released by the phosphor per unit of radiation exposure. Dosimeters have to be chosen according to the purpose of dosimetry. For example, $CaSO_4:Dy$ is 80% more sensitive than $LiF:Mg,Ti$, whereas $LiF:Mg,Cu,P$ is 60% more sensitive than $LiF:Mg,Ti$. So, for personnel dosimetry a $LiF:Mg,Ti$ is used. For patient dosimetry in diagnostic radiology and radiotherapy practices $LiF:Mg,Cu,P$ TLDs are recommend. For quality assurance practice $CaSO_4:Dy$ are ideal [36, 37].

A thermoluminescence system (detector-reader-annealing processes-irradiation) presents a good reproducibility of heating cycles during the read out process, which is important for accurate dosimetry [36]. Finally, one of the most essential characteristics of TLDs is their energy independence. The energy response of TLDs to high energy photon beam and low energy photon beam is similar for any certain dose. For this reason, they are ideal for a variety of practices.

2.4.3 Read-out and annealing process

In order to understand the read-out process of TLDs, it is important to understand the reading system used to evaluate TLDs. A basic TLD reader system consists of: a planchet for placing and heating the TLD, a photomultiplier tube (PMT) to detect the thermoluminescence light emission and convert it into an electrical signal linearity, proportional to the detected photon fluence, and an electrometer for recording the PMT signal as charge (see: **Fig. 2.4.4**).

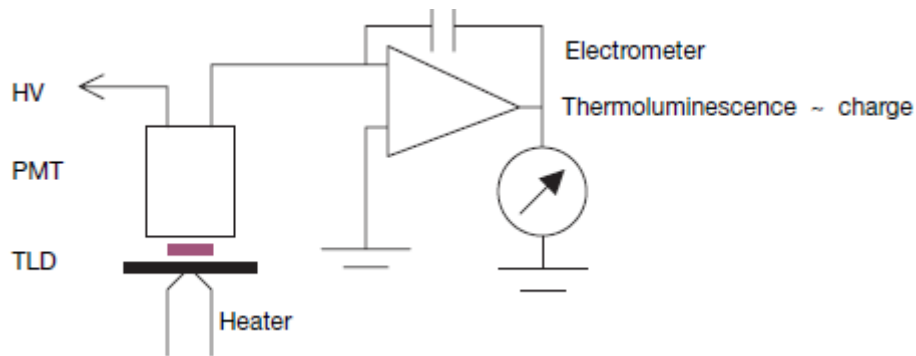


Fig. 2.4.4 TLD reader

The thermoluminescence intensity emission is a function of the TLD temperature. Keeping the heating-rate constant makes the temperature proportional to time and so the thermoluminescence intensity can be plotted as a function of time (or temperature). The resulting curve is called the TLD glow curve. TLDs have multiple trap depths and each trap depth gives a different glow peak. After a peak, there is a rapid fall-off of the thermoluminescence intensity due to charge carrier release. Thus, the thermoluminescence peak is not symmetric. The height of the crystal glow curve peaks depends on the depth of each trap. This means that traps of lower depths will be observed in lower temperature levels. These peaks have a short half-life, resulting to higher fading. These peaks can be removed by pre-heating just before the read-out (annealing). After the TLDs are read-out, they are annealed again in order to ensure the signal has been completely removed and the TLD is again ready for use. [33, 34].

For instance, for LiF:Mg, Ti detectors the annealing process consists of heating to 400 °C for 60 minutes before irradiation and then they are annealed for 2 hours at 100°C following by heating to 80 °C for 60 minutes after irradiation [37]. After this process the main dosimetry peak will remain at the glow curve (see: Fig. 2.4.5).

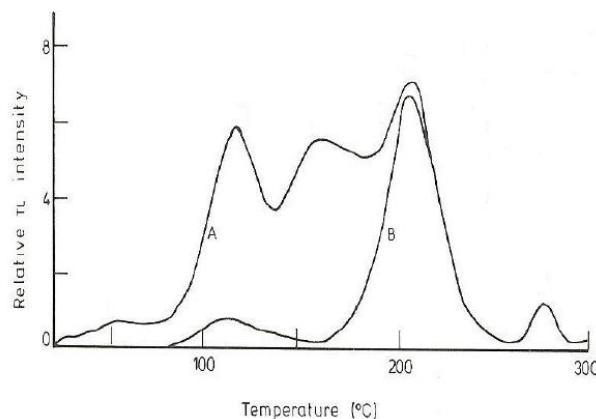


Fig. 2.4.5 Glow curves from LiF:Mg, Ti. (A) Glow curve without annealing, (B) Glow curve with annealing [38]

2.4.4 TLDs' Calibration

The calibration of TLDs is performed to correlate the read-out of signal process with the absorbed dose. In most cases, for industry needs, routine calibrations are performed using ^{137}Cs or ^{60}Co , reference beams. Therefore, TLD's are irradiated in well

known radiation fields. Because of this, for each TLDs' signal from read-out process there is a value of absorbed dose. Then, the calibration curve is constructed where the TLDs' signal and absorbed dose are proportional. It is important that the dose must be verified with a well-calibrated reference instrument, such as an ionization chamber [34]. Nevertheless, according to J.M. Bordy et al. [39], in cases of the interventional radiology/cardiology procedures, a specific calibration using a reference beam with energy lower than 150 keV is suggested since it is useful to choose a quality close to the one frequently met at the workplace.

2.4.5 Element correction coefficient

Dosimeters of the same batch often differ greatly in their sensitivity. The sensitivity variance in a typical batch of TLDs is unavoidable, but can be reduced from 15-20% to 1-2% when the dosimeters are calibrated in known fields, in order to be given an individual correction factor. Through this process each TLD is given an element correction coefficient (ECC) which can be expressed by:

$$ECC_i = \frac{\langle Q \rangle}{Q_i}$$

Where,

- $\langle Q \rangle$ = The average measured charge of the calibration dosimeters
- Q_i = The measured charge of dosimeter i

The ECC is then multiplied with the response of each dosimeter and its sensitivity becomes identical to the mean of all the dosimeters.

2.5 Interventional radiology procedures

Interventional radiology is a medical sub-specialty of radiology utilizing minimally-invasive image-guided procedures to diagnose and treat various endovascular, cardiovascular and musculoskeletal diseases. The advantages of interventional radiology procedures are: fewer risks, lower cost, comfort, less recovery time needed and better health outcomes compared to open surgery. This master thesis focuses on the measurements of three general categories of interventional procedures **i) angioplasty, ii) Embolization/chemoembolization and iii) Vertebroplasty procedures.**

2.5.1 Angiography and angioplasty

The Peripheral Arterial Disease (PAD) is a condition where plaque builds up in the arteries that carry blood to the head, organs, and limbs. Plaque is made up of fat, cholesterol, calcium, fibrous tissue, and other substances in the blood. When plaque builds up in the body's arteries, the condition is called atherosclerosis. Over time, plaque can harden and narrow the arteries, which limit the flow of oxygen-rich blood to the organs and other parts of the body. PAD usually affects the arteries in the legs, but it also can affect the arteries that carry blood from your heart to your head, arms, kidneys, and stomach.

The treatment for this disease is the angioplasty or stenting, which are procedures used for the treatment of a narrow or blocked artery. This is achieved with the use of either a balloon to stretch the artery (angioplasty) or a metal scaffold to hold the artery open (stent). These procedures improve blood flow which helps to relieve any symptoms the patient experience. All these procedures are performed without incisions or any other damage to the skin, through a small pin hole puncture.

2.5.2 Embolization/Chemoembolization

Cutting off the blood supply to a specific area of the body, can be an important form of care when treating tumors (or other abnormal growths), internal bleeding and aneurysms. Embolization is an invasive surgical procedure, which cuts off the blood flow of the affected area. The interventional radiologist inserts a catheter (small plastic tube) through a primary artery and propel it to the area where the blood supply needs to be cut off. The specialists inject a granulated or particulate material that congeals and hardens, thus blocking the blood flow or they may insert a metallic coil through the catheter, which remains in place, so the body will form a blood clot around the coil and block off the area. The materials used may depend on the size and type of the area which is to be closed and on whether the occlusion is intended to be temporary or permanent. Apart from these techniques, in the case of liver cancer treatment, the physician may inject small embolic particles, coated with chemotherapeutic drugs, through a catheter and into an artery, directly supplying the tumor. These particles can both block the blood supply and induce cytotoxicity, attacking the tumor in several ways. This procedure is called chemoembolization.

2.5.3 Vertebroplasty

Vertebroplasty is considered an image-guided spinal procedure in which bone cement is injected through a small hole of the skin (percutaneously) and into a fractured vertebra, with the goal of relieving back pain, caused by vertebral compression fractures. It is a minimally invasive procedure and the patients usually go home on the same or the next day of the procedure. The patients are administered with local anesthesia and light sedation for the procedure, though it can be performed by using only local anesthetic, for patients with medical problems, who cannot tolerate sedatives. During the procedure, bone cement is injected with a biopsy needle into the collapsed or fractured vertebra, which is maneuvered with fluoroscopic x-ray guidance. The cement (most commonly PMMA, although more modern cements are used as well) quickly hardens and forms a supportive structure within the vertebra, that provides stabilization and strength. The needle makes a small puncture on the patient's skin, which is easily covered with a small bandage after the procedure.

3 Materials and methods

3.1 Protocol

All the measurements were conducted at the 2nd Department of Radiology at "Attikon" General University Hospital. All the procedures were performed using a C-arm fluoroscopic system Toshiba infinix VC-i, with 30 cm x 40 cm flat panel detector (see: Fig. 3.1.1).

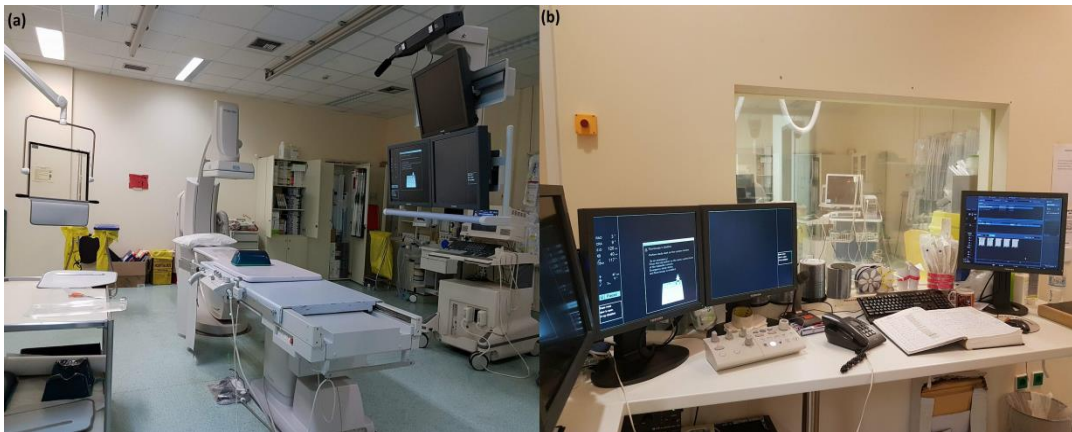


Fig. 3.1.1 (a) Fluoroscopic system Toshiba infinix VC-i, (b) C-arm console

The study included 98 interventional radiology (IR) procedures for the assessment of the occupational eye lens and brain doses from three general categories: **i)** Angiographies and angioplasties Lower Limbs (DSA- Digital Subtraction Angiography/PTA- Percutaneous Transluminal Angioplasty LL-Lower Limb) (N=70), **ii)** Embolization/chemoembolization procedures (N=15) and **iii)** Vertebroplasty procedures (N=13). The selection criteria of these IR procedures were: **i)** the high radiation dose per procedure and **ii)** the highest frequency of each procedure according to radiology department archives. Two groups of interventional radiologists participated in this study. The first group performed DSA/PTA LL and Embolization/Chemoembolization procedures and consisted of four physicians. The second group performed Vertebroplasty procedures and consisted of two physicians. The measurements were performed with MTS-N TLDs (LiF: Mg, Ti).



Fig. 3.1.2 TLDs positioning during IR procedures

A set of 7 dosimeters was attached to each physician for each procedure. In total, 84 TLDs were used (70 for the assessment of the occupational dose and 14 for the calculation of background dose). Four TLDs were placed on the radiologist's forehead: one dosimeter on the left side of the temple, one over the left eyebrow, one over the right eyebrow and one on the right side

of the temple. Moreover, 3 TLDs were placed on the physician's lead-glasses, so they would not be shielded by them: two dosimeters were placed on the upper two corners of the lead-glasses' frame (right and left) and one in the middle (see: **Fig. 3.1.2**).

The measurement process lasted approximately 4 months (November 2017 - March 2018). The reading of the dosimeters was carried out once all the measurements had been conducted. Afterwards, the doses per procedure were calculated, for each region where the dosimeters were placed.

Radiation doses were calculated as following:

- The dose per procedure for the forehead's right side was calculated as the average dose per procedure of the right temple and the right eyebrow.
- The dose per procedure for the forehead's left side was calculated as the average dose per procedure of the left temple and the left eyebrow.
- The dose per procedure for the left eye was calculated as the average (dose per procedure) of the dosimeters placed on the middle and the left corner of the radiologist's lead glasses.
- The dose per procedure of the right eye was calculated, as the average (dose per procedure) of the dosimeters placed on the middle and the right eye of the radiologist's lead glasses.

Dose report and parameters like DAP, type of the procedure, physician's experience, the distance of the flat panel from the patient, the time of exposure for each interventional radiologist and the use of protective equipment were recorded for all the procedures.

3.2 Interventional radiologists' behavior

The interventional radiologists' behavior in the interventional suite should also be considered, as it might significantly influence the measurements of the received doses. Such behavior includes their positioning during the procedures, the protective devices used and the distance between the flat panel detector and the patient.

The protective equipment that was used from the first group was: lead shielding ceiling, table lead curtain, mobile floor screen, lead apron, lead glasses and thyroid collar. In contrast, the second group did not use lead shielding ceiling, but they used lead gloves and non-lead radiation protective cup. During the DSA/PTA LL and Embolization/Chemoembolization procedures the first group of interventional radiologists placed the flat panel in the minimum possible distance from the patient, whereas during the Vertebroplasty procedures the second group placed the flat panel in a long distance from the patient. During the Embolization/Chemoembolization procedures the assistant interventional radiologist was not on the right side of the primary operator, as usual, but in several cases he was standing on his left side. Finally, both interventional radiologists' groups were standing behind the mobile floor screen during the cine acquisition.

3.3 TLDs management

For the purpose of this study, 84 MTS-N (TLD-100) were used. The shape of TLDs was a solid disk pallet with 4.5 mm diameter and 0.89 mm thickness. They are made from Lithium Fluoride doped with Magnesium and Titanium (LiF:Mg,Ti). The code name MTS with the additional symbol, represents the isotopic content of Lithium. In this case, N represents natural abundance (^6Li -7.5%, ^7Li 92.5 %).

Form	solid disc 4.5 mm diameter, of selected thickness
Effective atomic number Z	8.2
Density [g.cm ⁻³]	2.5
TL emission spectrum [nm]	400
Relative sensitivity to TLD-100	1.5
Main peak temperature [oC]	210
Zero dose reading [mGy]	15
Detection threshold [mGy]	10
Linearity range [Gy]	5×10 ⁻⁵ - 5
Repeatability	< 2%
Photon energy dependence 30 keV - 1.3 MeV	< 30 %
Batch homogeneity [1 SD]	< 5 %
Thermal fading [% at room temperature]	< 5% / yr
Fluorescent light effect on fading and zero reading	negligible at laboratory light intensity
Reusability	unlimited
Dose rate influence	independent

Fig. 3.3.1The main feature of MTS-N pallets

The MTS-N are ideal detectors for personal dosimetry, due to their atomic number which is close to the atomic number of human tissue ($Z_{\text{eff}}=8.2$ and $Z_{\text{eff}}=7.4$, respectively). Also, their small size makes them suitable for point measurements as they do not disturb the radiation field. Moreover, MTS-N detectors are reusable and they present large range linearity between TLD signal and dose (see chapter 2.4.2). For easier recognition, all TLDs were inserted into custom-made cases with their code number printed on the cases. The TLDs (with their cases) that were used for the head dose evaluation were attached onto headbands (see: **Fig. 3.3.2**)



Fig. 3.3.2 A set of 7 TLDs that were used on this study

3.3.1 Element correction coefficient (ECC)

Dosimeters of the same batch that have been irradiated with the same uniform dose and the same geometrical conditions, show different sensitivity (see: **chapter 2.4.5**). For this reason, it is necessary to calculate the Element Correction Coefficient (ECC) for each batch of TLD, which will be used to correct the read-out process's measurements. Concerning the measurement of ECC, all TLD disks that were used in this study were placed into TLD slide (four in each slide) and then the slides were placed into special dosimeter cards (TLD slide holder). Finally, all dosimeter cards were loaded into cassettes (20 cards in each cassette) (see: **Fig 3.3.3**) and every cassette was placed in an irradiator of a ⁹⁰Sr radioactive source (see: **Fig 3.3.4**).

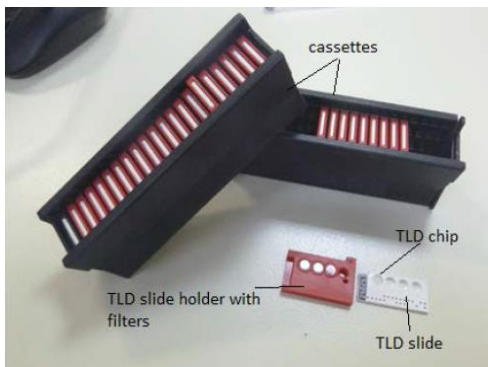


Fig. 3.3.3 TLD cassettes with their cases



Fig. 3.3.4 ⁹⁰ Sr irradiator

All TLDs were irradiated with the same dose. Afterwards, the TLDs' average signal was calculated based on their readings. In the end of this process all TLDs were annealed. This process was repeated further two times. The ECC_{ji} was calculated for each TLD as follows:

$$ECC_{ji} = \frac{\langle Q_j \rangle}{Q_{ji}}$$

Where,

- $\langle Q_j \rangle$ = Average signal of TLDs for each process
- Q_{ji} = The signal of each TLD for each process

Therefore, the aforementioned process generated 3 ECC values for each TLD, so the final ECC for each TLD is the average of each TLD's 3 values.

$$ECC_i = \frac{(\sum_{j=1}^3 ECC_{j,i})}{3}$$

In order for a TLD to be reliable for diagnostic radiology dosimetry, it needs to present a good repeatability. The repeatability is expressed by the Coefficient of Variation (CV), which for each TLD is derived from standard deviation (SD) relative to the final ECC for each TLD.

$$CV = \frac{SD}{ECC_i} \cdot 100\%$$

In diagnostic radiology dosimetry, the CV's accepted limit for each TLD must be less than 5%. In this case, all the TLDs that were used, presented a CV from 0.15% to 3.52%. Therefore, all TLDs included in the study, were reliable. The calculation process of the ECC was held at the Department of Dosimetry and Calibration of the Greek Atomic Energy Commission (GAEC).

3.3.2 TLDs annealing

Before irradiation, all TLD disks were annealed for 1 hour at 400°C in a special oven (WEST 4100+, RadPro International, see: **Fig. 3.3.5.a**), followed by fast cooling-down to room temperature. Then the TLD's were annealed for 2 hours at 100°C, in order to reset their signal (see: **chapter 2.4.3**). For the annealing procedure the thermoluminescent material was placed on tray of stainless steel (see: **Fig. 3.3.5.b**), which fit in the oven.

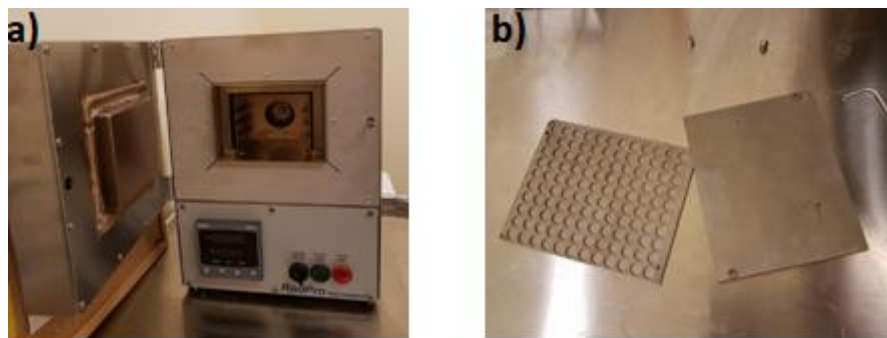


Fig. 3.3.5 a) West 4100+ Oven, b) Tray of stainless street

3.3.3 TLDs read-out process

The read-out process of TLDs was performed at the Department of Dosimetry and Calibration of the GAEC. The TLDs readings were performed using a Mirion RE 2000 reader (see **Fig. 3.3.8**). The reader was connected to a computer where the readings were processed by a software called RADOS TLD SERVER. Similarly to the calculation process of the ECC, all TLDs were installed into dosimeter cards which were placed into cassettes. The cassettes were fed into the reader automatically by a conveyor. Every slide was pushed out of dosimeter card into to the reader, and the TLD disk was then lifted from the slide into the measuring chamber where it was heated by hot nitrogen. Slides from dosimeter cards are changed automatically after all of the TLD disks in the slide had been measured. The reader's temperature was increasing exponentially up to 300 °C in order to obtain the maximum of the dosimeter's emitted light. The total signal of a TLD reading procedure is shown in the glow curve below (see: **Fig. 3.3.7**).

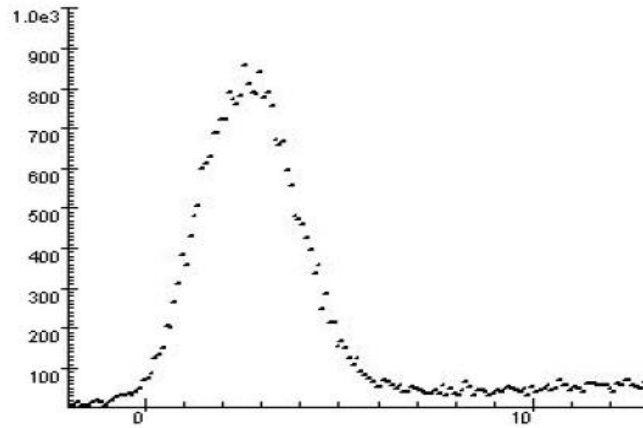


Fig. 3.3.6 TLD glow curve after pre-heated annealing

Before the read-out process, the TLD's were pre-heated at 80°C for 1 hour in order to erase the signal from low-temperature peaks (see: **chapter 2.4.3**). The oven that was used for the annealing was a Thermo Scientific's Heraeus (see: **Fig. 3.3.9**). Afterwards, all TLDs signals were collected and corrected. The correction applied to the TLDs signals, is defined as follows:

$$\text{TLDs signal}_{\text{corrected},i} = (\text{TLDs signal}_{\text{read-out},i}) \cdot \text{ECC}_i - \text{Ave. TLDs signal}_{\text{Background}}$$

Where,

$$\text{Ave. TLDs signal}_{\text{Background}} = \frac{\sum_{i=1}^N (\text{TLD signal}_{\text{Background},i}) \cdot \text{ECC}_i}{N}$$

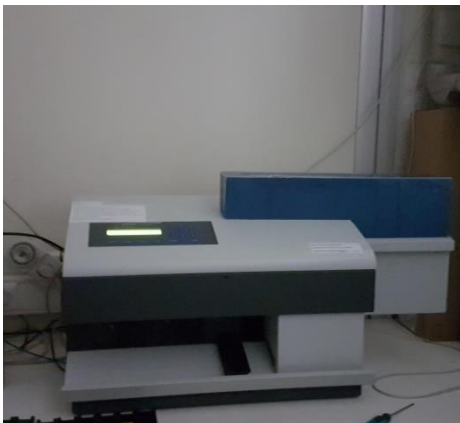


Fig. 3.3.7 Mirion RE 2000 reader



Fig. 3.3.8 Thermo Scientific's Heraeus oven

3.3.4 Calibration

The TLDs' calibration was performed at the Ionizing Radiation Calibration Laboratory (IRCL) of the GAEC, which is a Secondary Standard Radiation Calibration Laboratory (SSDL). A total of, eleven TLDs were separated in two groups. The group A (N=6) was separated in two subgroup of three and each subgroup received a dose of 1mSv. The group B (N=5) was also separated in two subgroup of three and two and each subgroup received a dose of 2mSv. TLDs were irradiated with the PANTAK x-ray tube (see: **Fig. 3.3.10**).



Fig. 3.3.9 PANTAK X-ray tube at the Ionizing Radiation Calibration Laboratory of the Greek Atomic Energy Commission

All TLDs were placed into custom-made cases and then were attached into headbands, in order to simulate the experiment's conditions. Then the band of TLDs was placed around a water-filled cylindrical phantom with a diameter and height of 20 cm, while the lateral wall thickness was 0.5 cm (see: **Fig.3.3.11**). The cylindrical phantom was made of polymethylmetacrylat (PMMA) and was selected in order to better stimulate the human head [40]. The qualities of the radiation (x-tube voltage and 1st HVL) were selected based on RQR quantities, as the energy range and the less-filtered radiation, that characterize fluoroscopically guided procedures, are closer to the RQR series energy range [41]. The calibration was based on the RQR-9. The adjustments used for the calibration process were according to the IEC 61267 for the RQR-9: x-ray tube voltage set on 120 kVp and 1st HVL set on 5 mm of Aluminum [39].

TLDs were calibrated in terms of $H_p(3)$, in order to determine the eye lens dose of interventional radiologists. In order to determine the head dose, $H_p(3)$ was converted to $H_p(0.07)$ According to, Behrens R. et al. [42] the conversion factor from $H_p(3)$ to $H_p(0.07)$ for calibration to cylindrical phantom and energy photons above 30 keV is approximately 0.85 (see: **Table 3.3.1**).

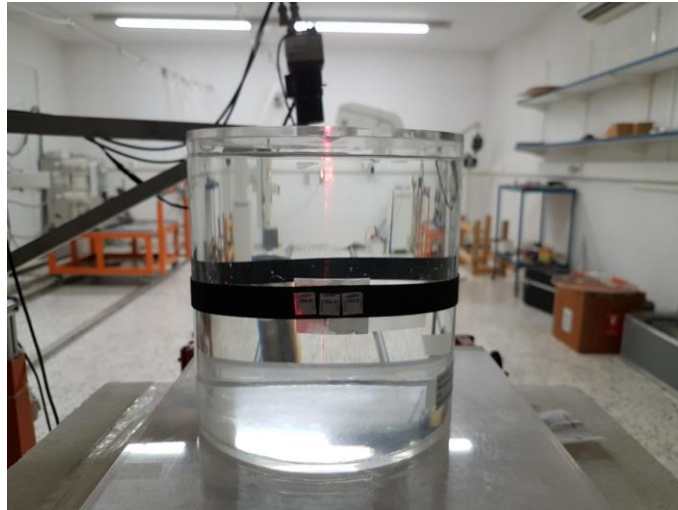


Fig. 3.3.10 Cylindrical PMMA phantom with TLD's band.

After the TLDs' irradiation an annealing process, of 80°C for 1 hour was performed, to erase any undesirable signals. The equipment used consisted of: a Thermo Scientific's Heraeus oven (annealing process), a Mirion RE 2000 reader (read-out process) and the RADOS TLD SERVER software (TLD reading). Finally, all TLDs signals were obtained and their values corrected with the ECCs. Two calibration curves were designed, one for the assessment of eye lens dose and the other for the assessment of head dose (see: Fig 3.3.12-3.3.13).

Table 3.3.1 Corrected signal with corresponded dose for eyes and head, respectively [43]

Group of TLDs	TLDs corrected signal	Hp(3) (mSv)	Hp(0.07) (mSv)
A	18235	1	0.85
	19900	1	0.85
	22624	1	0.85
	20747	1	0.85
	23383	1	0.85
	21942	1	0.85
B	49152	2	1.7
	48635	2	1.7
	48228	2	1.7
	43558	2	1.7
	44237	2	1.7

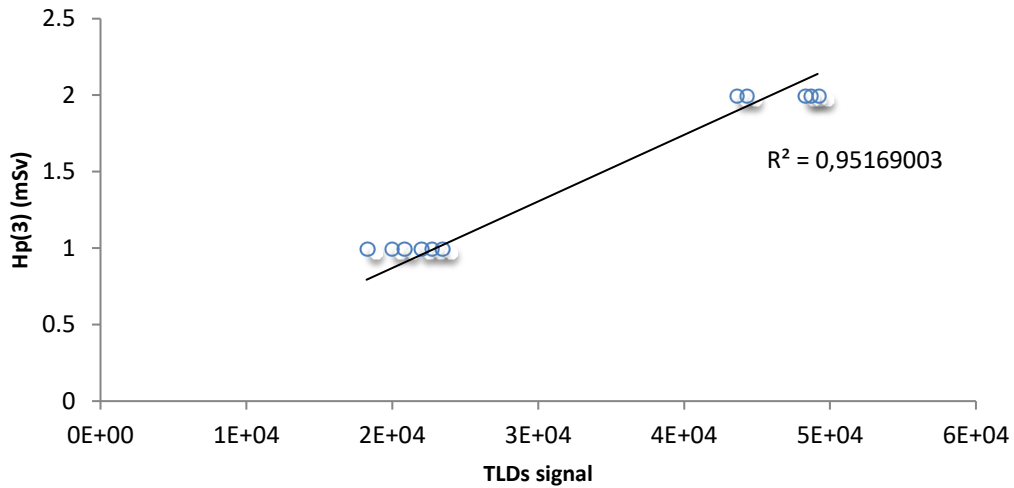


Fig. 3.3.11 Calibration curve for the eye lens

The linear relationship between the eye lens dose and the TLDs corrected signal, according to the above graph, is:

$$y = 0.00004352 \cdot x$$

Where,

- $y = \text{Dose}_{\text{eye lens}} \text{ (m Sv)}$
- $x = (\text{TLDs signal}_{\text{read-out},i}) \cdot \text{ECC}_i - \text{Avarage TLDs signal}_{\text{Background}}$

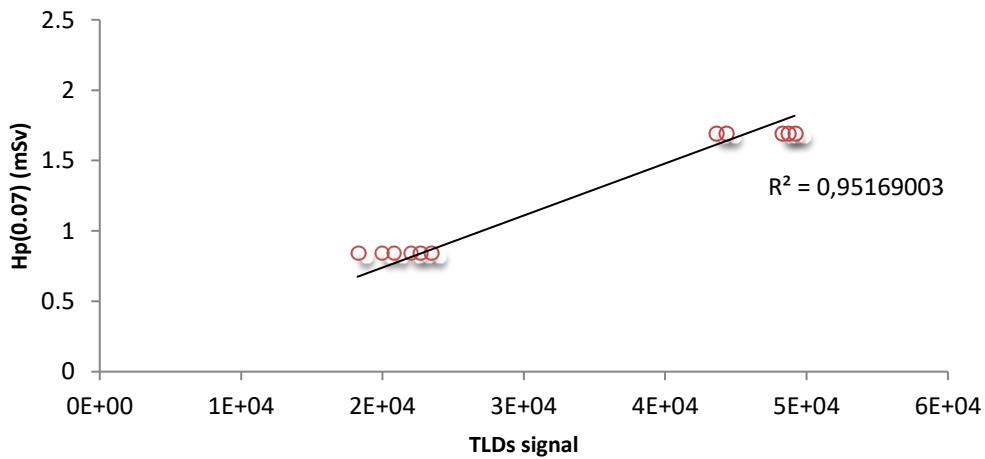


Fig. 3.3.12 Calibration curve for the head

The linear relationship between the head dose and the TLDs corrected signal, according to the above graph, is:

$$y = 0.00003699 \cdot x$$

Where,

- $y = \text{Dose}_{\text{head}} \text{ (m Sv)}$
- $x = (\text{TLDs signal}_{\text{read-out},i}) \cdot \text{ECC}_i - \text{Avarage TLDs signal}_{\text{Background}}$

3.4 Data analysis

SPSS software v. 23 ((SPSS, Inc., Chicago, IL, USA) was used for the statistical analysis and the assessment of data's normality. Since our sample was less than 50 values, Shapiro-Wilk test was adopted to check the data's normality. The non-parametric Wilcoxon signed-rank test was performed to demonstrate whether there was a statistically significant difference between the doses per procedure, in the anatomic regions of interest. Pearson and Spearman correlation coefficient were used to investigate any possible correlations between the dose per procedure, in each anatomic region, and the interventional radiologist's experience. In all cases, a level of $p=0.05$ was defined as statistically significant

Furthermore, Microsoft excel 2007 was used for the estimation of the doses per procedure received by each anatomic region. Also, it was used for constructing the calibration curves and for detecting any possible presence of linear relationships between the dose per procedure, in the eye lens (right and left) and the forehead (right and left side), for all types of procedures.

4 Results

4.1 Interventional radiologists' profile

The interventional radiologists' profile can influence the received dose. Their profile, in the period of this study, includes: their experience over the years, the total number of procedures performed, the total time of exposure for each interventional radiologist and their positioning during the procedure. The results for each interventional radiologist are shown on the **Table 4.1.1**. In the first group, of 4 interventional radiologists, all the participants in the DSA/PTA LL procedures were primary operators, whereas in the embolization/chemoembolization procedures only one was a primary operator and the rest participated as assistants. In the second group, of 2 interventional radiologists, one was a primary operator and the other was an assistant operator to all of the procedures.

Table 4.1.1 Interventional radiologists' profile

Type of procedure	Interventional radiologist #	Experience (in years)	Number of procedures (during the study)	Total time of exposure (min)	Interventional radiologist's position
DSA/PTA LL	1	26	13	106.7	P
	2	12	19	261.6	P
	3	8	21	354.9	P
	4	6.5	17	188.7	P
Embolization/ Chemoembolization	1	26	15	252.1	P
	2	12	5	76.8	A
	3	8	8	102.6	A
	4	6.5	3	24.9	A
Vertebroplasty	5	18	13	286.5	P
	6	9	12	259.4	A

P=Primary operator, A=Assistant operator

4.2 DSA/PTA LL procedures

In this type of procedures all the interventional radiologists were primary operators. The average doses per procedure for each position of TLDs and each interventional radiologist, are displayed on **Table 4.2.1**. It is observed that the interventional radiologist 1 received lower radiation dose than the other three interventional specialists. Also, it is detected that the TLDs' positioned on the left side of the head (left temple, over left eyebrow and left upper corner of lead-glasses), for all operators, received higher radiation dose than the TLDs' positioned on the right side of the head (right temple, over right eyebrow and right upper corner of lead-glasses).

Table 4.2.1 Dose per procedure for each position of TLDs' position in DSA/PTA LL procedures

Type of procedure	TLDs' position	Interventional radiologist			
		1 (P)	2 (P)	3 (P)	4 (P)
DSA/PTA LL	Right Temple	12.2	17.1	6.5	16.8
	Over Right Eyebrow	19.5	25.7	15.5	35.4
	Over Left Eyebrow	22.6	42.9	36.7	45.3
	Left Temple	20.6	49.3	46.4	50.6
	Right Upper Corner of the Lead-glasses	14.7	40.8	26.3	21.8
	Middle of the Lead-glasses	49.3	55.8	69.1	73.5
	Left Upper Corner of the Lead-glasses	40.7	66.6	70.4	77.9

The dose per procedure for each anatomic region of interest and for each interventional radiologist was calculated following the protocol described in **chapter 3.1**. The results are presented on **Table 4.2.2**. It is clear that the left side of the head received higher dose than right side, on all occasions. Moreover, the anatomic region which received the higher dose was the left eye, for all the operators. The highest value of dose per procedure was detected in interventional radiologist 4, on the lens of the left eye (75.7 μ Sv).

Table 4.2.2 Received dose per procedure per anatomic region, in DSA/PTA LL procedures

Type of procedure	Anatomic region	Interventional radiologist			
		1 (P)	2 (P)	3 (P)	4 (P)
DSA/PTA LL	Forehead's right side	15.9	21.4	11.0	26.1
	Forehead's left side	21.6	46.1	41.6	48.0
	Lens of the right eye	32.0	48.3	47.7	47.6
	Lens of the left eye	45.0	61.2	69.7	75.7

4.3 Embolization/Chemoembolization procedures

The average doses per procedure for each position of the TLDs, are shown on **Table 4.3.1**. In these cases, only the interventional radiologist 1 was a primary operator whereas all the others acted as assistants to all the procedures. A remarkable result is that the dose per procedure for two of the assistant operators, is higher than the primary operator's. Usually, the primary operator receives higher dose than the assistant. As in DSA/PTA LL procedures, TLDs' positioned on the left side of the head received higher radiation dose than those positioned on the right side of the head, for all radiologists.

Table 4.3.1 Dose per procedure for each TLDs' position in Embolization/Chemoembolization procedures

Type of procedure	TLDs' position	Interventional radiologist			
		1 (P)	2 (A)	3 (A)	4 (A)
Embolization/ Chemoembolization	Right Temple	20.0	57.8	20.2	52.5
	Over Right Eyebrow	26.3	70.4	23.9	46.5
	Over Left Eyebrow	48.1	73.0	43.6	128.7
	Left Temple	64.3	79.6	36.9	171.7
	Right Upper Corner of the Lead-glasses	31.7	92.7	25.1	80.6
	Middle of the Lead-glasses	75.7	122.9	51.8	199.7
	Left Upper Corner of the Lead-glasses	77.5	107.0	55.5	195.0

The doses per procedure, for each anatomic region of interest, in embolization/chemoembolization procedures are presented on **Table 4.3.2**. The dose per procedure received by interventional radiologist 1, who was a primary operator on both types of procedures, is higher on the embolization procedures than the DSA/PTA LL procedures. The same trend is also observed on the rest operators, but it cannot be compared since their position in the procedures was different (assistant and primary respectively). As in DSA/PTA LL procedures, the anatomic region which received higher dose was the left eye, for all the operators. The highest dose per procedure was observed in interventional radiologist 4 on the lens of the left eye (197.3 μ Sv).

Table 4.3.2 Received dose per procedure per anatomic region, in Embolization/Chemoembolization procedures

Type of procedure	Anatomic region	Interventional radiologist			
		1 (P)	2 (A)	3 (A)	4 (A)
Embolization/ Chemoembolization	Forehead's right side	23.2	64.1	22.0	49.5
	Forehead's left side	56.2	76.3	40.3	150.2
	Lens of the right eye	53.7	107.8	38.5	140.2
	Lens of the left eye	76.6	114.9	53.6	197.3

4.4 Vertebroplasty procedures

The average doses per procedure for each position of the TLDs, are demonstrated on **Table 4.4.1**. In this type of procedures, one of the interventional radiologists was a primary operator and the other one was an assistant. The primary operator received higher dose per procedure than the assistant. As in the other two types of procedures, the TLDs' positioned on the left side of the head, received higher radiation dose than the TLDs' positioned on the right side of the head.

Table 4.4.1 Dose per procedure of TLDs' position in Vertebroplasty procedures

Type of procedure	TLDs' position	Interventional radiologist	
		5 (P)	6 (A)
Dose (μSv) per procedure			
Vertebroplasty	Right Temple	116.5	143.3
	Over Right Eyebrow	492.3	283.0
	Over Left Eyebrow	1359.4	454.8
	Left Temple	1644.0	473.1
	Right Upper Corner of the Lead-glasses	551.3	183.0
	Middle of the Lead-glasses	1760.6	499.5
	Left Upper Corner of the Lead-glasses	1762.7	478.5

The dose per procedure for each anatomic region of interest in vertebroplasty procedures, are presented on **Table 4.4.2**. It is observed that this type of procedure delivers the highest radiation burden to interventional radiologists, among the other types of procedures examined in this study. In vertebroplasty procedures, the highest value of dose per procedure was detected in interventional radiologist 5 on the lens of the left eye (1761.6 μSv), which is the highest value of dose per procedure encountered in this study.

Table 4.4.2 Received dose/pro per anatomic region, in Vertebroplasty procedures

Type of procedure	Anatomic region	Interventional radiologist	
		5 (P)	6 (A)
Dose (μSv) per procedure			
Vertebroplasty	Forehead 's right side	304.4	213.2
	Forehead 's left side	1501.7	464.0
	Lens of the right eye	1155.9	341.2
	Lens of the left eye	1761.6	489.0

4.5 Radiation dose from IR procedures

The dose per procedure in relation to the type of procedure and the interventional radiologists' positioning (primary or assistant) for each anatomic region, is displayed on the following histograms (see: Fig. 4.5.1- 4.5.4). According to the histograms, DSA/PTA LL procedures present the lowest level of radiation burden, whereas the vertebroplasty procedures have the highest. The primary operator of vertebroplasties receives the highest scatter dose. Also, the lens of the left eye and the forehead's left side, are the anatomic regions with the highest radiation exposure. The most remarkable finding is that the assistant operator of embolizations/ chemoembolizations receives less radiation than the primary.

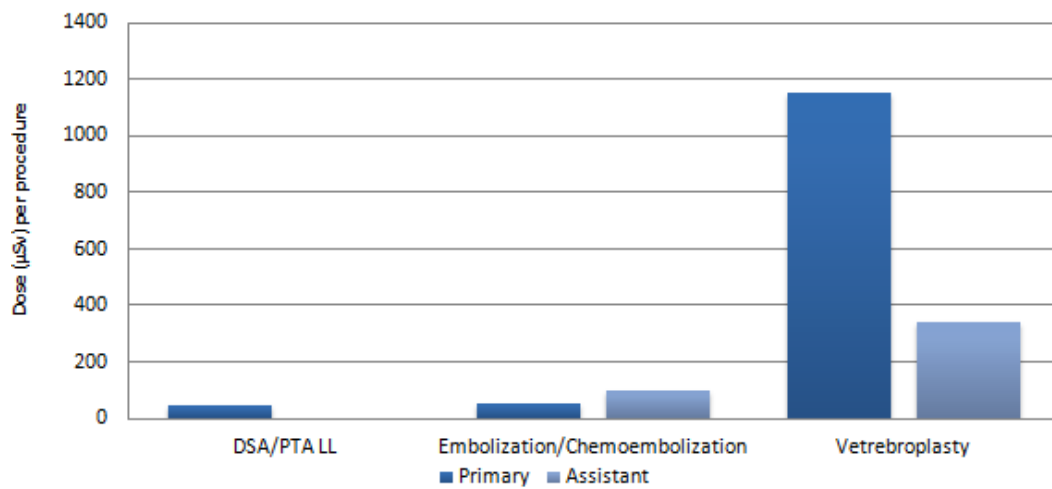


Fig. 4.5.1 Dose per procedure for the lens of the right eye

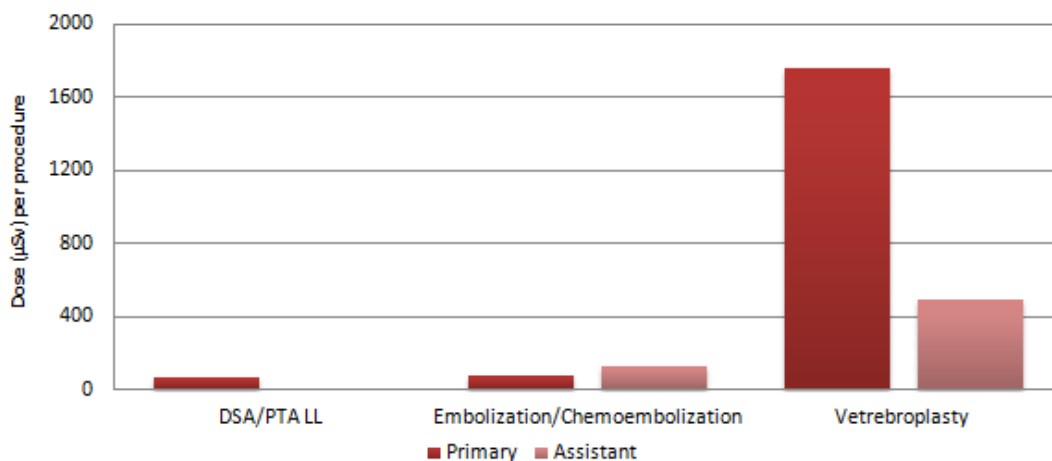


Fig. 4.5.2 Dose per procedure for the lens of the left eye

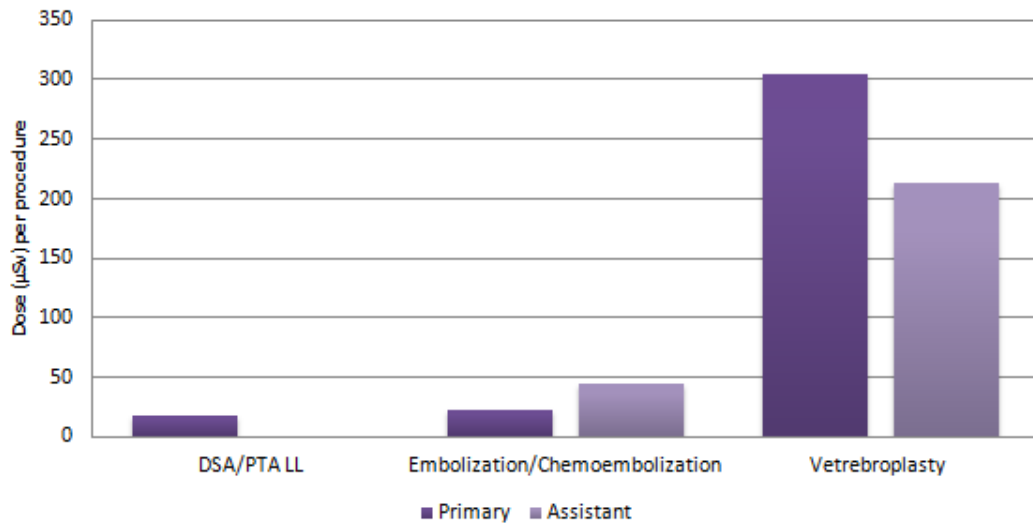


Fig. 4.5.3 Dose per procedure for the forehead's right-side

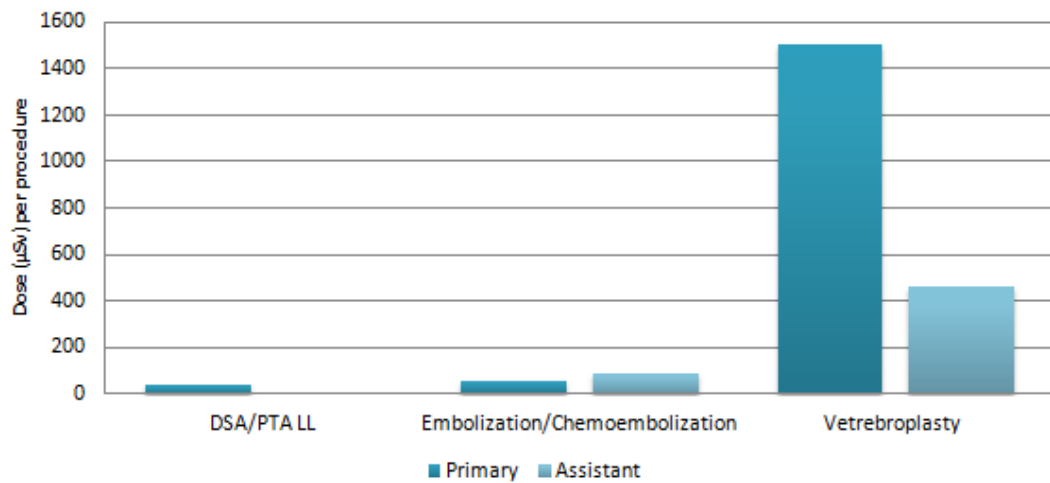


Fig. 4.5.4 Dose per procedure for the forehead's left-side

4.6 Estimation of the annual dose

The assessment of the annual doses is important in order to investigate if any of the interventional radiologists exceeded the new annual dose limit for the lens of eyes. The calculation of the annual doses was based on the annual workload of each interventional radiologist for each type of procedure. The number of procedures performed by each interventional radiologist in relation to the interventional radiologists' position during the year 2017 is presented on **Table 4.6.1**. The annual workload was recorded from the interventional radiology department's logbook.

Table 4.6.1 Annual workload during 2017

Type of procedure	Interventional radiologist #	Number of procedures during 2017	Interventional radiologist's position
DSA/PTA LL	1	86	P
	2	113	P
	3	92	P
	4	71	P
Embolization/ Chemoembolization	1	83	P
	2	23	A
	3	32	A
	4	37	A
Vertebroplasty	5	15	P
	6	15	A

The estimated annual dose for each interventional radiologist were determined by multiplying the average dose per procedure, for each anatomic region, with the annual workload. The following tables present the calculated annual doses, on both forehead's sides and eye lenses, for the interventional radiologists who performed DSA/PTA LL and Embolization/ Chemoembolization procedures (see Tables 4.6.2 & 4.6.3) and for the interventional radiologists who performed Vertebroplasty procedures (see Table 4.6.4).

Table 4.6.2 Interventional radiologists' annual doses in DSA/PTA LL procedures

Type of procedure	Anatomic region	Interventional radiologist			
		1 (P)	2 (P)	3 (P)	4 (P)
DSA/PTA LL	Forehead's right side	1.4	2.4	1.0	1.9
	Forehead's left side	1.9	5.2	3.8	3.4
	Lens of the right eye	2.8	5.5	4.4	3.4
	Lens of the left eye	3.9	6.9	6.4	5.4

Table 4.6.3 Interventional radiologists' annual doses in Embolization/Chemoembolization procedures

Type of procedure	Anatomic region	Interventional radiologist			
		1 (P)	2 (P)	3 (P)	4 (P)
Embolization/ Chemoembolization	Forehead's right side	1.9	1.5	0.7	1.8
	Forehead's left side	4.7	1.8	1.3	5.6
	Lens of the right eye	4.5	2.5	1.2	5.2
	Lens of the left eye	6.4	2.6	1.7	7.3

Table 4.6.4 Interventional radiologists' annual doses in Vertebroplasty procedures

Type of procedure	Anatomic region	Interventional radiologist	
		5 (P)	6 (A)
Vertebroplasty	Forehead's right side	4.6	3.2
	Forehead's left side	22.5	7.0
	Lens of the right eye	17.3	5.1
	Lens of the left eye lens	26.4	7.3

4.7 Correlation of DAP-Dose per procedure

The DAP values per procedure for each interventional radiologist in DSA/PTA LL procedures, are displayed on **Table 4.7.1**. The DAP per procedure was calculated as the average DAP of all the procedures performed by each radiologist. It is observed that the DAP per procedure is higher for interventional radiologist 1 than the other three operators ($79.1 \pm 28 \text{ Gy}\cdot\text{cm}^2$).

Table 4.7.1 DAP per procedure, DAP range for each operator in DSA/PTA LL procedures

Interventional radiologist	DAP (Gy·cm ²) per procedure mean±SD	DAP (Gy·cm ²) range
1 (P)	79.1 ±28	2.1-339.8
2 (P)	25.5±6.9	1.9-103.9
3 (P)	35.5±14.6	2.1-246.3
4 (P)	55.7±16.9	4.2-199.9

The linear relationship between DAP per procedure and occupational dose per procedure was investigated on the following figures (see: **Fig 4.7.1-4.7.4**). The results showed that there is no linear relationship between DAP and the radiation dose in any anatomic regions.

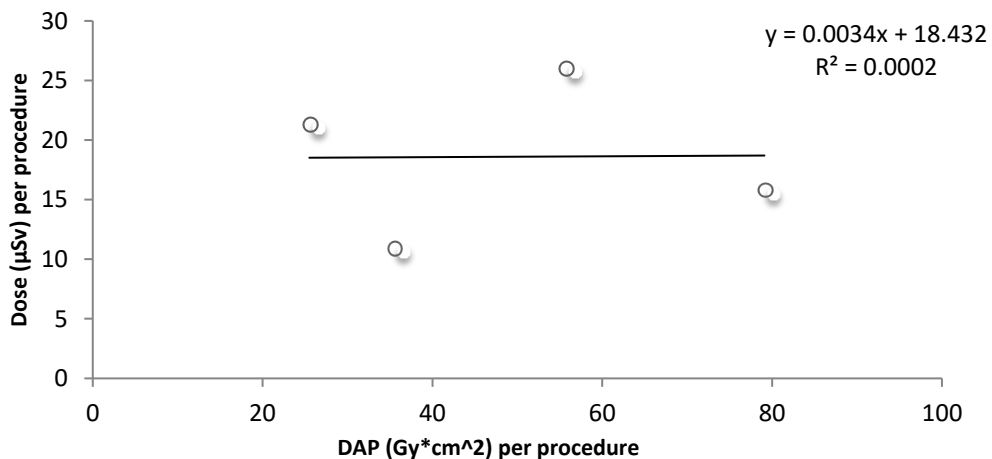


Fig. 4.7.1 Correlation between DAP and occupational dose the forehead's right side

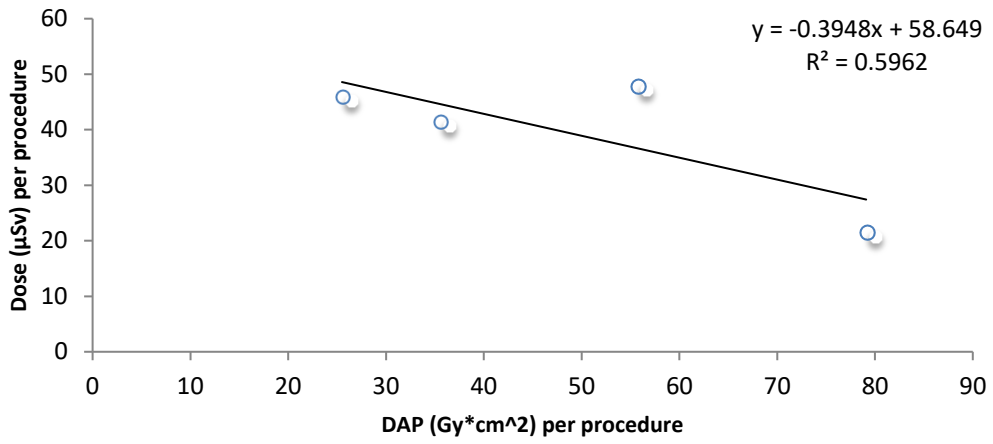


Fig. 4.7.2 Correlation between DAP and occupational dose on the forehead's left

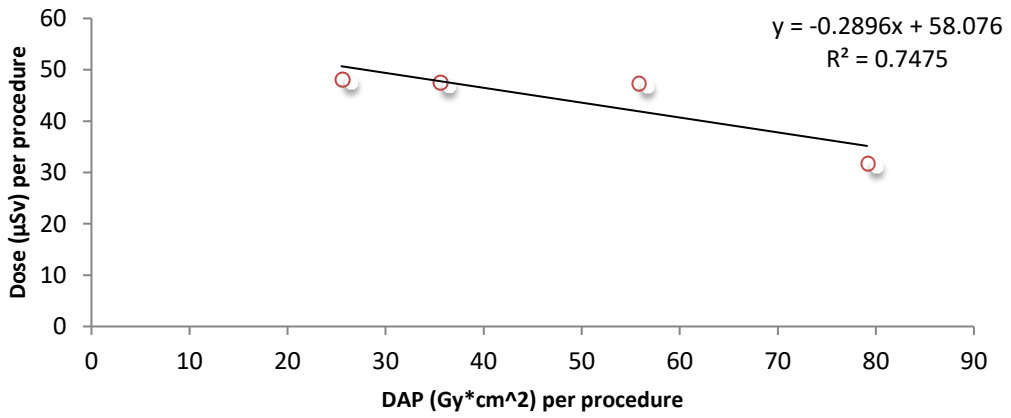


Fig. 4.7.3 Correlation between DAP and occupational dose on the lens of the right eye

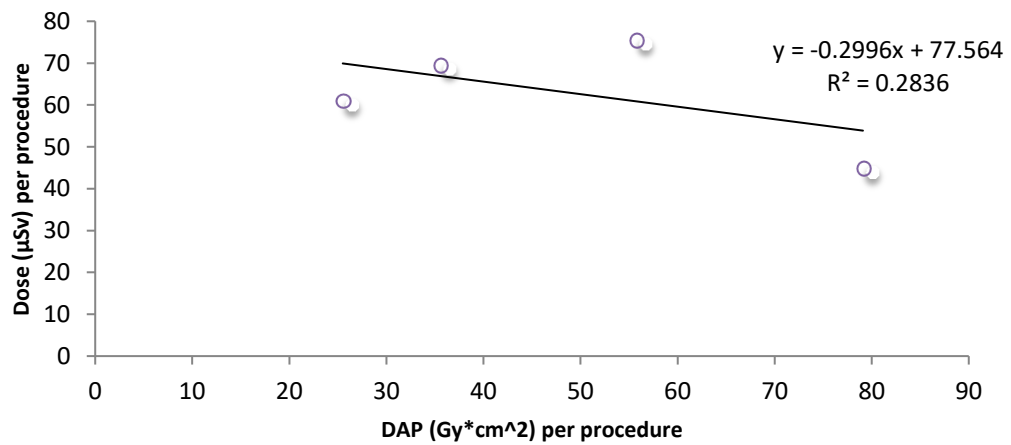


Fig. 4.7.4 Correlation between DAP and occupational dose on the lens of the left eye

4.8 Statistical analysis of the doses per procedure for the anatomic regions of interest

Before reviewing whether there was a statistically significant difference between the dose to the various anatomic regions, it was essential to check whether the data distribution is normal. Shapiro-Wilk test was used for the data's normality assessment (see Table 4.8.1). The results showed that none of the variable distributions is normal.

Table 4.8.1 Normality test 1

	Shapiro-Wilk		
	Statistic	df	Sig.
Dose_per_procedure_on_the_left_eye_lens	,530	10	,000
Dose_per_procedure_on_the_right_eye_lens	,546	10	,000
Dose_per_procedure_on_the_left_side_of_the_forehead	,540	10	,000
Dose_per_procedure_on_the_right_side_of_the_forehead	,666	10	,000

Therefore, the non-parametric Wilcoxon signed-rank test was used to demonstrate whether there was a statistically significant difference between the dose per procedure on the following anatomic regions:

- Lens of the right eye lens vs. lens of the left eye lens,
- Forehead's right side vs. Forehead's left side,
- Lens of the right eye vs. Forehead's right side and
- Lens of the left eye vs. Forehead's left side.

The dose per procedure was calculated as the total average dose derived from all the 6 radiologists participated in the study, for all the types of IR procedures. The results are presented on **Table 4.8.2**. It was founded that the dose per procedure on the lens of the left eye was statistically significantly higher than the dose on the lens of the right eye and the forehead's left side. Also, the dose per procedure on the lens of the right eye was statistically significantly higher than the dose on the forehead's right side. Regarding the forehead's levels, the dose per procedure on the left side was statistically significantly higher than the dose on the right side.

Table 4.8.2. Results of the Wilcoxon signed-rank test. The significance level was 0.05

Variables of interest	p-value
Dose per procedure on the lens of the left eye vs. Dose per procedure on the lens of the right eye	0.005
Dose per procedure on the forehead's left side vs. Dose per procedure on the forehead's right side	0.005
Dose per procedure on the lens of the left eye vs. Dose per procedure on the forehead's left side	0.005
Dose per procedure on the lens of the right eye vs. Dose per procedure on the forehead's right side	0.005

4.9 Statistical analysis of the correlation of doses per procedure and the operator's experience

The normality test for the dose per procedure for each anatomic region of interest and the operators' years of experience, are displayed on the **Table 4.9.1**. The aforementioned parameters concern the first group of interventional radiologists performed DSA/PTA LL procedures. The results show that all distributions are normal except for the dose per procedure on the lens of the right eye.

Table 4.9.1 Normality Test 2

	Shapiro-Wilk		
	Statistic	df	Sig.
Dose_per_procedure_on_the_left_eye_lens_DSA_PTA_LL	,950	4	,718
Dose_per_procedure_on_the_right_eye_lens_DSA_PTA_LL	,666	4	,004
Dose_per_procedure_on_the_left_side_of_the_forehead_DSA_PTA_LL	,810	4	,122
Dose_per_procedure_on_the_right_side_of_the_forehead_DSA_PTA_LL	,987	4	,944
Experience_years	,834	4	,179

Therefore, the correlation between the interventional radiologists' experience and the dose per procedure, during DSA/PTA LL procedures, on the lens of the left eye, the forehead's left side and the forehead's right side, was based on the Pearson correlation coefficient. On the other hand, the correlation between the interventional radiologists' experience and the dose per procedure on the lens of the right eye, in DSA/PTA LL procedures, was calculated based on the Spearman correlation coefficient. The correlation results are demonstrated on **Table 4.9.2**. A negative strength correlation (P.C.=-0.979) was observed between the interventional radiologists' experience and the dose per procedure on the lens of the left eye lens.

Table 4.9.2 Correlation's results between the doses per procedure and the interventional radiologist's experience

Variable vs. Experience's years	Correlation coefficient	p-value
Dose per procedure on the lens of the left eye	-0.979 (P.C.)	0.021
Dose per procedure on the lens of the right eye	-0.200 (S.C.)	0.800
Dose per procedure on the forehead's left side	-0.943 (P.C.)	0.057
Dose per procedure on the forehead's right side	-0.278 (P.C.)	0.722

P.C.=Pearson Correlation, S.C.=Spearman Correlation

4.10 Linear relationship of the dose per procedure on the eyes and the forehead

The linear relationship between the dose per procedure on the lens of the left and right eye with the forehead's left and right side, is presented on the following graphs. In **Fig. 4.10.1**, it is observed that the dose per procedure on the forehead's left side is reduced by a factor of 0.85, in regard to the lens of the left eye.

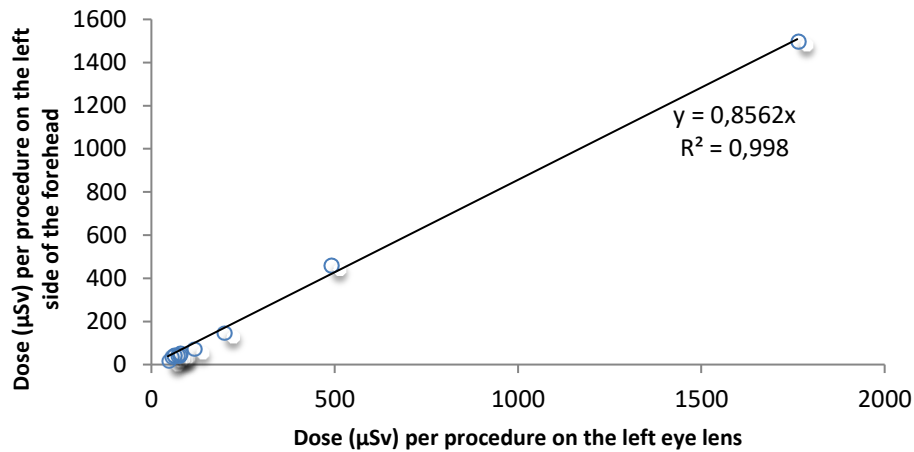


Fig. 4.10.1 Linear relationship between the dose per procedure on the forehead's left side and the lens of the left eye

According to **Fig. 4.10.2**, the dose per procedure on the right side of the head is reduced by a factor of 0.30, in relation to the lens of the right eye.

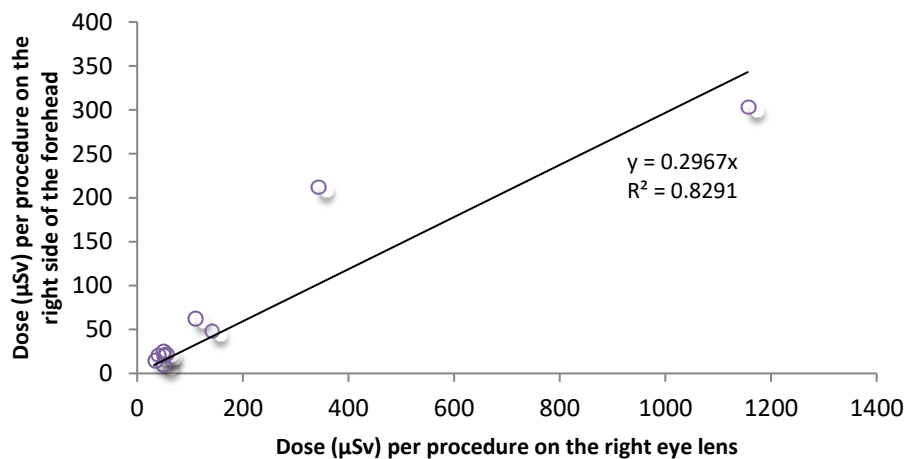


Fig. 4.10.2 Linear relationship between the dose per procedure on the forehead's right side and the lens of the right eye

5 Discussion

This master thesis concluded on some interesting results. Between the three types of the examined IR procedures (DSA/PTA LL, Embolizations/Chemoembolizations and Vertebroplasties), we found that vertebroplasty procedures deliver the highest values of radiation burden to both primary and assistant operators. One possible explanation is that the interventional radiologists chose not to use the lead shielding ceiling and place the flat panel at the highest possible distance from the patient, as it was more convenient for them to perform the procedure. According to Qianjun Jia, et al. [43], the use of lead shielding ceiling can significantly reduce the received scatter radiation dose to interventional radiologists. The study showed that when the lead shielding ceiling was placed close to the patient, the reduction was 76.8 %, for the primary operator, and 81.9 % when it was placed at the left lateral position. The most efficient position was close to the primary operator, where the reduction was 93.5 %. The corresponding results for the assistant operator were 70.3 %, 76.7 % and 90.0 %, respectively. Also, one more explanation, that vertebroplasties presented the highest radiation levels, is that they are very complex procedures and therefore, they require prolonged fluoroscopy time.

The statistical analysis concluded that the dose per procedure on the lens of the left eye and the forehead's left side were significantly higher than the corresponding doses per procedure on the right side. The most probable explanation is that the left side of the interventional radiologists is closer to the X-ray tube than the right side and as a result it is more exposed to radiation. Furthermore, it was observed that the doses per procedure on the eye lenses were significantly higher than the corresponding doses on the forehead's sides. This is a reasonable outcome, as the forehead's distance from the x-ray source is larger than the eye lens's and due to the inverse square law, the forehead receives lower dose than the eye lenses.

The correlation between the interventional radiologists' experience (in years) with the received doses per procedure, for each anatomic region of interest, in DSA/PTA LL procedures showed that there is a negative strength correlation (Pearson correlation coefficient = - 0.979) between the dose per procedure and the physician's experience on the lens of the left eye . Only the DSA/PTA LL procedures were chosen, since in that type of procedure, all the operators were primary. This finding is attributed to the fact that the most experienced interventional radiologist completed the procedures in a shorter-time (see table 4.1.1), The correlations between the physician's experience and the dose per procedure on the right side of the head (lens of the right eye and forehead's right side) did not present any statistical significance. This may be attributed to the to uncertainty of the low-dose measurements. A non-significance difference was observed between the experience and the forehead's left and right side.

Moreover, no linear relationship was observed between DAP and dose per procedure, which can be explained by the use of room shielding and each operator's distance from the radiation source. According to Reeves, R.R., et al. [20], the operators' position may affect his/her exposure, when indicators such as fluoroscopy time and DAP are similar. Additionally, the RadiCure study found that fluoroscopy time and DAP were not significantly reduced compared with the operators' exposure reduction [44].

On the other side, some studies demonstrated a linear relationship between the DAP and the adsorbed dose, however, they were not performed under clinical conditions. In the aforementioned study, the scatter doses were measured with solid state detectors, positioned at a fixed distance from the radiation source, and PMMA phantoms to simulate the patients. Therefore, this finding is linked with the fixed distance the “operators” had from the radiation source. Also, the distance between the flat-panel and the patient-phantom, the fluoroscopy pulses, the acquisition rate, the field size and the collimation were the same during the experiments. [31, 45, 46].

An unusual finding reported in Embolizations/Chemoembolizations. In this type of procedures, the dose per procedure was higher to the assistant than the primary operator. The assistant operator is usually on the right side of the primary operator and due to the inverse square law, he/she receives lower dose than the primary. Nonetheless, in several cases in this study, during Embolization/Chemoembolization procedures, the assistant operator was standing on the primary’s left side and therefore, he received higher doses.

An interesting finding is the strong linear relationship between the dose per procedure on the lens of the left and the right eye with the forehead’s left and right side, respectively. R^2 was 0.998 between the lens of the left eye and the forehead’s left side and 0.829 for the right side, respectively. As a result, the linear relationship between the dose to eye lens and the dose to the forehead (for the same side) allows us to estimate the dose to the eye lens when the dose to the forehead is known and the reverse.

Recently, the ICRP provided recommendations for the new occupational annual dose limit for the eye lens and the threshold for radiation-induced cataract. These changes were performed, after several studies raised concerns regarding the previous annual dose limit to the eye lens for occupational exposure, and the threshold for radiation-induced cataract [47]. The previous annual dose limit for the eye lens was 150 mSv, in terms of equivalent dose, and the threshold for detectable lens opacities, was 5 Sv for chronic exposure, 0.5-2.0 Sv for acute exposure, 8 Sv for fractional exposure and 5 Sv for acute exposure for visual impairment (cataract) [17]. The new threshold for cataract formation is 0.5 Sv and the new occupational annual dose limit is 20 mSv, in average for a 5-year period, with no single year exceeding 50 mSv [5].



Fig. 4.10.1 Annual dose without considering the lead-glasses’ shielding

In this master thesis, we estimated the annual doses received by the interventional radiologists' eye lenses. On the above histogram (see: **Fig. 4.10.1**) displays the estimated annual doses on the lens of the right and left eye, for both interventional radiologist groups, in comparison with the new annual limit.

As observed in the figure above, the annual dose of the interventional radiologist 5 on the lens of the left was the only case where the annual limit was exceeded. However, it is important to emphasize that the TLDs were placed on the physician's lead-glasses, so they weren't shielded by them. Therefore, the above estimation of the annual doses on the operators' eye lenses ignores the lead-glasses shielding. According to Gebel et al., who studied the transmission factor from eight different radiation protection eyewear models, when the scattered radiation strikes the lead-glasses from the front, they have the same effect on both the right and left eye, and only small differences could be seen between the different models. The transmission factors, that Gebel et al. calculated, ranged from 13 to 27 % [46]. The following histogram (see: **Fig. 4.10.2**), demonstrates the estimation of the annual doses on the eye lenses for both interventional radiologist groups considering the lead-glasses shielding. The transmission factor used for the correction of the measurements was 27%. In this case, none of the interventional radiologists exceed the eye lenses annual limit.

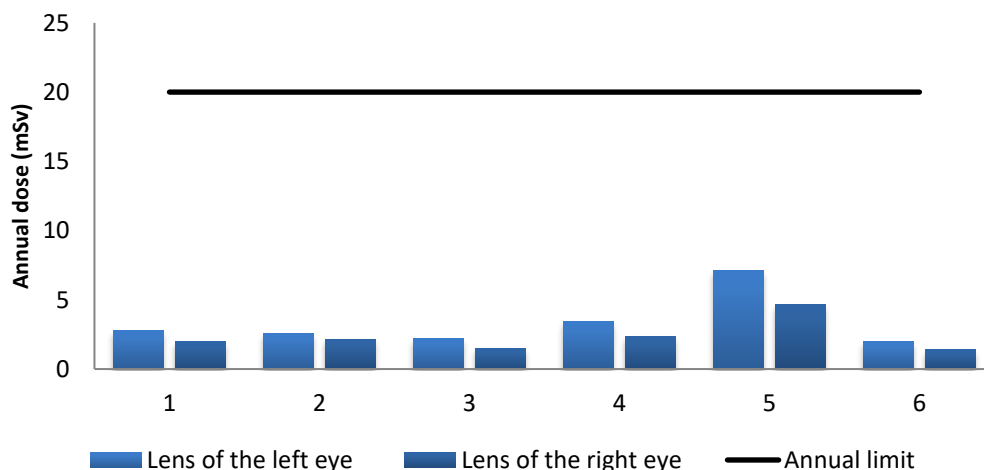


Fig. 4.10.2 Annual dose considering the lead-glasses' shielding

Table 4.10.1 presents the results of other relevant studies, for the three types of procedures examined. The values present the doses per procedure on the lens of the left eye for the primary operator. In DSA/PTA LL procedures, our results are very similar to the literature with the exception of two cases. A probable reason is that they preferred to use the median value to estimate the dose per procedure. In Embolizations/Chemoembolizations the results of this master thesis are in accordance with the literature. Finally, in Vertebroplasty procedures, a considerable difference is observed between this study and the literature. This can be attributed to the different protocols used among the various studies. For example, Fitousi, N.T., et al. [48] considered the shielding from the ceiling suspended screen, whereas Von Wrangel, A., A.

Cederblad, and M. Rodriguez-Catarino [49] in order to estimate the dose per procedure on the eye lens placed the dosimeter on the physician's forehead.

Table 4.10.1 Values' comparison with other related studies

Study	DSA/PTA LL	Embolization/ Chemoembolization	Vertebroplasty
	Dose (μ Sv) per procedure		
Current study	63 (Average value)	77 (Average value)	1762 (Average value)
Domienik, J., et al. [32]	15 (Median value)	85 (Median value)	-
Nikodemová, D., et al. [50]	13 (Median value)	60 (Median value)	-
Efstathopoulos, E.P., et al. [51]	-	-	1129 (Maximum value)
Ciraj-Bjelac, O. and M.M. Rehani [52]	16-64 (Range)	15-66 (Range)	-
Bacchim Neto, F.A., et al. [53]	53.7 (Median value)	-	-
Vanhavere F., C.E., Gualdrini G., Clairand I., et al. [54]	20 (Median value) 52 (Average value)	80 (Median value) 120 (Average value)	-
Fitousi, N.T., et al. [48]	-	-	328* (Average value)
Von Wrangel, A., A. Cederblad, and M. Rodriguez-Catarino [49]	-	-	230** (Average value)

6 Conclusion

The purpose of current master thesis was the evaluation of the occupational doses per procedure on the eyes lenses and the forehead's sides in three categories of interventional radiology procedures (DSA/PTA LL, Embolizations/Chemoembolization and Vertebroplasties).

Overall, the highest levels of radiation burden were recorded on Vertebroplasty procedures both to the primary and assistant operator. Also, we found significantly higher dose per procedure on the lens of the left eye and the forehead's left side than on the lens of the right eye and forehead's right side. Furthermore, the doses per procedure on the eye lenses were significantly higher than the corresponding doses per procedure on the forehead's sides. One interesting finding was the strong negative correlation between the interventional radiologists' experience (in years) and the dose per procedure on the left eye lens in DSA/PTA LL procedures. Also, we found a linear relationship between the dose per procedure on the left and right eye lenses with the forehead's left and right side, respectively. This can be considered a good indicator for estimating the dose on the forehead's side if we only know the dose on the respective eye lens and the opposite.

The no-use of the appropriate radiation protection tools lead to surpassing of the dose limits. In particular, when the use of the ceiling suspended screen is impossible, the operators must be obligated to wear lead-glasses to avoid the exceeding of the annual dose limit (20 mSv) to the their eyes' lenses.

References

1. Valentin, J., *Avoidance of radiation injuries from medical interventional procedures*. Ann ICRP, 2000. **30**(2): p. 7-67.
2. Chodick, G., et al., *Risk of cataract after exposure to low doses of ionizing radiation: a 20-year prospective cohort study among US radiologic technologists*. Am J Epidemiol, 2008. **168**(6): p. 620-31.
3. Picano, E., et al., *Cancer and non-cancer brain and eye effects of chronic low-dose ionizing radiation exposure*. BMC Cancer, 2012. **12**: p. 157.
4. Roguin, A., et al., *Brain and neck tumors among physicians performing interventional procedures*. Am J Cardiol, 2013. **111**(9): p. 1368-72.
5. Authors on behalf of, I., et al., *ICRP publication 118: ICRP statement on tissue reactions and early and late effects of radiation in normal tissues and organs--threshold doses for tissue reactions in a radiation protection context*. Ann ICRP, 2012. **41**(1-2): p. 1-322.
6. *The 2007 Recommendations of the International Commission on Radiological Protection*. ICRP publication 103. Ann ICRP, 2007. **37**(2-4): p. 1-332.
7. Shigematsu, N., et al., *Nuclear Disaster after the Earthquake and Tsunami of March 11*. The Keio Journal of Medicine, 2012. **61**(1): p. 28-34.
8. Koenig, T.R., et al., *Skin injuries from fluoroscopically guided procedures: part 1, characteristics of radiation injury*. AJR Am J Roentgenol, 2001. **177**(1): p. 3-11.
9. Administration., U.S.F.a.D., *Electronic products; performance standard for diagnostic xray systems and their major components*. . Federal Register 2005. **70**(11).
10. Miyake, H. and et al., *[Medical electrical equipment - part 2-43: particular requirements for the basic safety and essential performance of X-ray equipment for interventional procedures]*. Nihon Hoshasen Gijutsu Gakkai Zasshi, 2011. **67**(3): p. 298-301.
11. Balter, S. and D.L. Miller, *Patient skin reactions from interventional fluoroscopy procedures*. AJR Am J Roentgenol, 2014. **202**(4): p. W335-42.
12. Jacob, S., et al., *Occupational cataracts and lens opacities in interventional cardiology (O'CLOC study): are X-Rays involved? Radiation-induced cataracts and lens opacities*. BMC Public Health, 2010. **10**: p. 537.
13. Ciraj-Bjelac, O., et al., *Risk for radiation-induced cataract for staff in interventional cardiology: is there reason for concern?* Catheter Cardiovasc Interv, 2010. **76**(6): p. 826-34.
14. Shore, R.E., K. Neriishi, and E. Nakashima, *Epidemiological studies of cataract risk at low to moderate radiation doses: (not) seeing is believing*. Radiat Res, 2010. **174**(6): p. 889-94.
15. Ainsbury, E.A., et al., *Radiation cataractogenesis: a review of recent studies*. Radiat Res, 2009. **172**(1): p. 1-9.
16. Seals, K.F., et al., *Radiation-Induced Cataractogenesis: A Critical Literature Review for the Interventional Radiologist*. Cardiovasc Intervent Radiol, 2016. **39**(2): p. 151-60.
17. ICRP, *ICRP Publication 60. 1990 Recommendations of the International Commission on Radiological Protection*. Ann. ICRP 1991.
18. Nakashima, E., K. Neriishi, and A. Minamoto, *A reanalysis of atomic-bomb cataract data, 2000-2002: a threshold analysis*. Health Phys, 2006. **90**(2): p. 154-60.
19. Hammer, G.P., et al., *Occupational exposure to low doses of ionizing radiation and cataract development: a systematic literature review and perspectives on future studies*. Radiat Environ Biophys, 2013. **52**(3): p. 303-19.
20. Reeves, R.R., et al., *Invasive Cardiologists Are Exposed to Greater Left Sided Cranial Radiation: The BRAIN Study (Brain Radiation Exposure and Attenuation During Invasive Cardiology Procedures)*. JACC Cardiovasc Interv, 2015. **8**(9): p. 1197-1206.

21. Roguin, A., J. Goldstein, and O. Bar, *Brain tumours among interventional cardiologists: a cause for alarm? Report of four new cases from two cities and a review of the literature*. *EuroIntervention*, 2012. **7**(9): p. 1081-6.
22. finkelstein, M., *Is brain cancer an occupational disease of cardiologists?* *The Canadian journal of cardiology* 1998.
23. Darby, S.C., et al., *Radiation-related heart disease: current knowledge and future prospects*. *Int J Radiat Oncol Biol Phys*, 2010. **76**(3): p. 656-65.
24. Plummer, C., et al., *Ischemic stroke and transient ischemic attack after head and neck radiotherapy: a review*. *Stroke*, 2011. **42**(9): p. 2410-8.
25. Loganovsky, K., *Do Low Doses of Ionizing Radiation Affect the Human Brain?* *Data Science Journal*, 2009. **8**: p. BR13-BR35.
26. Vano, E., et al., *Eye lens exposure to radiation in interventional suites: caution is warranted*. *Radiology*, 2008. **248**(3): p. 945-53.
27. Koukorava, C., et al., *Doses to operators during interventional radiology procedures: focus on eye lens and extremity dosimetry*. *Radiat Prot Dosimetry*, 2011. **144**(1-4): p. 482-6.
28. Albayati, M.A., et al., *Editor's choice--Angulation of the C-arm during complex endovascular aortic procedures increases radiation exposure to the head*. *Eur J Vasc Endovasc Surg*, 2015. **49**(4): p. 396-402.
29. IAEA. *Radiation protection of medical staff in interventional fluoroscopy*. Available from: <https://www.iaea.org/resources/rpop/health-professionals/interventional-procedures/radiation-protection-of-medical-staff-in-interventional-fluoroscopy>.
30. Vano, E., et al., *Influence of patient thickness and operation modes on occupational and patient radiation doses in interventional cardiology*. *Radiat Prot Dosimetry*, 2006. **118**(3): p. 325-30.
31. Vano, E., et al., *Staff radiation doses in interventional cardiology: correlation with patient exposure*. *Pediatr Cardiol*, 2009. **30**(4): p. 409-13.
32. Domienik, J., et al., *Extremity and eye lens doses in interventional radiology and cardiology procedures: first results of the ORAMED project*. *Radiat Prot Dosimetry*, 2011. **144**(1-4): p. 442-7.
33. *Radiation oncology physics: A handbook for teachers and students*, in *Radiation oncology physics: A handbook for teachers and students*, E.B. Podgorsak, Editor. 2005, IAEA: Vienna, 2005. p. 71-88.
34. *Clinical Dosimetry Measurements in Radiotherapy*. Medical Physics Monograph. 2009: Medical Physics Publishing.
35. Santos, L.A.P., et al., *Techniques for Measuring Some Characteristics of Ionizing Radiation Beams Using Bipolar Junction Transistor as a Detector*. 2013 3rd International Conference on Advancements in Nuclear Instrumentation, Measurement Methods and Their Applications (Animma), 2013.
36. Rivera, T., *Thermoluminescence in medical dosimetry*. *Appl Radiat Isot*, 2012. **71 Suppl**: p. 30-4.
37. Del Sol Fernandez, S., et al., *Thermoluminescent characteristics of LiF:Mg, Cu, P and CaSO₄:Dy for low dose measurement*. *Appl Radiat Isot*, 2016. **111**: p. 50-5.
38. McKinlay, A.F., *Thermoluminescence Dosimetry (Medical Physics Handbooks)*. 1981: CRC Press.
39. Bordy, J.M., et al., *Proposals for the type tests criteria and calibration conditions of passive eye lens dosimeters to be used in interventional cardiology and radiology workplaces*. *Radiation Measurements*, 2011. **46**(11): p. 1235-1238.
40. Gualdrini, G., et al., *A new cylindrical phantom for eye lens dosimetry development*. *Radiation Measurements*, 2011. **46**(11): p. 1231-1234.
41. Vanhavere F., C.E., Gualdrini G. , Clairand I., Sans Merce M., Ginjaume M., Nikodemova D., Jankowski J., Bordy J-M., Rimpler A., Wach S., Martin P., Struelens L., Krim S., Koukorava C., Ferrari P., Mariotti F., Fantuzzi E., Donadille L., Itié C., Ruiz N.,

- Carnicer A., Fulop M., Domienik J., Brodecki M., Daures J., Barth I.10, Bilski P., *ORAMED: Optimization of Radiation Protection of Medical Staff*. 2012.
42. Behrens, R. and G. Dietze, *Monitoring the eye lens: which dose quantity is adequate?* Phys Med Biol, 2010. **55**(14): p. 4047-62.
 43. Jia, Q., et al., *Operator Radiation and the Efficacy of Ceiling-Suspended Lead Screen Shielding during Coronary Angiography: An Anthropomorphic Phantom Study Using Real-Time Dosimeters*. Sci Rep, 2017. **7**: p. 42077.
 44. Christopoulos, G., et al., *Effect of a real-time radiation monitoring device on operator radiation exposure during cardiac catheterization: the radiation reduction during cardiac catheterization using real-time monitoring study*. Circ Cardiovasc Interv, 2014. **7**(6): p. 744-50.
 45. Leyton, F., et al., *Scatter radiation dose at the height of the operator's eye in interventional cardiology*. Radiation Measurements, 2014. **71**: p. 349-354.
 46. Geber, T., M. Gunnarsson, and S. Mattsson, *Eye lens dosimetry for interventional procedures – Relation between the absorbed dose to the lens and dose at measurement positions*. Radiation Measurements, 2011. **46**(11): p. 1248-1251.
 47. Thome, C., et al., *Deterministic Effects to the Lens of the Eye Following Ionizing Radiation Exposure: is There Evidence to Support a Reduction in Threshold Dose?* Health Phys, 2018. **114**(3): p. 328-343.
 48. Fitoussi, N.T., et al., *Patient and staff dosimetry in vertebroplasty*. Spine (Phila Pa 1976), 2006. **31**(23): p. E884-9; discussion E890.
 49. von Wrangel, A., A. Cederblad, and M. Rodriguez-Catarino, *Fluoroscopically guided percutaneous vertebroplasty: assessment of radiation doses and implementation of procedural routines to reduce operator exposure*. Acta Radiol, 2009. **50**(5): p. 490-6.
 50. Nikodemová, D., et al., *Staff extremity doses in interventional radiology. Results of the ORAMED measurement campaign*. Radiation Measurements, 2011. **46**(11): p. 1210-1215.
 51. Efsthopoulos, E.P., et al., *Occupational radiation doses to the extremities and the eyes in interventional radiology and cardiology procedures*. Br J Radiol, 2011. **84**(997): p. 70-7.
 52. Ciraj-Bjelac, O. and M.M. Rehani, *Eye dosimetry in interventional radiology and cardiology: current challenges and practical considerations*. Radiat Prot Dosimetry, 2014. **162**(3): p. 329-37.
 53. Bacchim Neto, F.A., et al., *Occupational radiation exposure in vascular interventional radiology: A complete evaluation of different body regions*. Phys Med, 2016. **32**(8): p. 1019-24.
 54. Vanhavere F., C.E., Gualdrini G., Clairand I., et al., *ORAMED: Optimization of Radiation Protection of Medical Staff*. 2012.